Pergamon

Progress in Oceanography 53 (2002) 57–103

Progress in Oceanography

www.elsevier.com/locate/pocean

The shallow overturning circulation of the Indian Ocean

Friedrich A. Schott *, Marcus Dengler, Rena Schoenefeldt

Institut für Meereskunde an der Universität Kiel, Düsternbrooker Weg 20, D-24105 Kiel, Germany

Abstract

The Indian Ocean differs from the other two large oceans in not possessing an annual-mean equatorial upwelling regime. While the subtropical cells (STCs) of the Atlantic and Pacific Oceans connect subtropical subduction regimes with tropical upwelling via equatorward thermocline flows and coastal undercurrents, much of the upwelling in the Indian Ocean occurs in the coastal regimes of the northern hemisphere. Consequently, the counterpart of the STCs of the other oceans has to be a cross-equatorial cell connecting the southern subtropical subduction zone via the Somali Current with the upwelling areas off Somalia and Oman. The southward return flow is by interior Ekman transports. This annual-mean picture is accomplished by a dominance of the summer monsoon, during which only northern upwelling occurs, over the winter monsoon. Pathways of the thermocline flows related to the shallow overturning circulations are investigated here and estimates of subduction and upwelling are presented. From the observed mean northward flow of thermocline waters within the Somali Current and the interior southward cross-equatorial return flow the magnitude of the cross-equatorial cell is estimated at 6 Sv, with part of the thermocline waters being supplied by the Indonesian Throughflow. From observations we estimate that the northern upwelling occurs dominantly through the offshore outflows of the Somali Current by the Southern Gyre and Great Whirl and to a lesser degree off Oman. However, we also present model results suggesting a much lower role of Somali upwelling and a significant contribution from open-ocean upwelling in cyclonic domes around India and Sri Lanka. An interesting aspect of the Indian Ocean cross-equatorial cell is the mechanism by which the Ekman transport crosses the equator. Typically, Ekman transports during the summer (winter) monsoon are southward (northward) on both sides of the equator, while mean meridional winds on the equator are in the respective opposite direction. Earlier model evidence had suggested that this type of forcing should lead to an equatorial roll with northward surface flow and southward subsurface flow during the summer monsoon and reverse orientation during the winter monsoon. Observational evidence is presented here, based on shipboard ADCP sections, moored stations and surface drifters, confirming the existence of the equatorial roll. It is strongly developed in the western Indian Ocean during the SW monsoon where the wind conditions for the roll are best met. While in the central Indian Ocean and during the winter monsoon the roll appears to be a more transient phenomenon, superimposed by equatorial-wave currents. The evidence further suggests that the roll is mostly confined to the surface-mixed layer and is, therefore, of little consequence for the meridional heat transport.

* Corresponding author. Tel.: +49-431-600-4100; fax: +49-431-600-4102.
E-mail address: fschott@ifm.uni-kiel.de (F.A. Schott).

0079-6611/02/$ - see front matter
PII: S0079-6611(02)00039-3

Contents

1. Introduction

While the shallow subtropical cells (STCs) of the Pacific and Atlantic connect subtropical subduction regimes via western-boundary undercurrents and interior thermocline recirculation with the equatorial

upwelling regimes from which the return flow to the subtropics is closed by poleward Ekman transports, the situation is quite different for the Indian Ocean. In the Indian Ocean, the Southeast Trades do not cross the equator, causing an equatorial divergence, but instead the annual-mean winds on the equator are eastward, causing a convergence on the equator (e.g. Schott & McCreary, 2001; henceforth called SM). Indian Ocean upwelling does not occur along the equator, but rather in the Northern Hemisphere, off Somalia, Oman and off India, and only during the summer monsoon.

The water upwelled off Somalia can be as cold as 16 °C, with densities in excess of 26.5 kg m^{-3}, out of a depth range of up to 300 m (e.g., Swallow & Bruce, 1966). These densities correspond to austral winter surface densities in the subtropics near 35°S. Typical upwelling temperatures and densities, as shown later for WOCE shipboard sections, appear to be more like 22 °C or 24.5 kg m^{-3}, respectively, corresponding to depths of about 100 m for the origin of the upwelled waters. On the other hand, as also discussed later, there are concerns that satellite surface temperatures may be biased high and thus suggest warmer upwelling than actually occurring (Vecchi et al., personal communication). The relatively low salinities of the water upwelled off Somalia clearly identify it as water originating from the Southern Hemisphere (Fischer, Schott, & Stramma, 1996). Hence, in the zonal-mean meridional circulation a shallow overturning cell is required with northward subsurface branches supplying the upwelling and southward surface branches, returning the upwelled water to the subduction region. Thus the Indian Ocean does not possess an STC but instead a cross-equatorial cell.

Subduction occurs dominantly in the southeastern subtropical Indian Ocean (Karstensen & Quadfasel, 2002; Zhang & Talley, 1998). Subducted water masses move westward in the South Equatorial Current (SEC), which splits, near 17°S, into the Northeast and the Southeast Madagascar Currents (e.g. Swallow, Fieux, & Schott, 1988; Fig. 1).

Within the SEC, subducted waters merge with waters originating in the Indonesian Throughflow regime. Consequently, part of the subducted water masses turn southward with the SE Madagascar Current, then into a retroflection zone at the southern end of Madagascar, from where there is partial return within the subtropical gyre and partial continuation towards the Agulhas Current (Fig. 1). The water masses passing westward past Cape Amber at the northern tip of Madagascar merge into the East African Coast Current (EACC) but a fraction also, as discussed subsequently, departs southward through the Mozambique Channel.

During the summer monsoon, from May to September, the EACC feeds into the cross-equatorial northward Somali Current flow which connects with the interior mainly through low-latitude outflow into the ‘Southern Gyre’. Upwelling occurs at the northern, offshore-turning flank of the Southern Gyre and the upwelled waters are carried far offshore. The offshore transport supplies cross-equatorial return flow southward, immediately offshore from the Somali Current (Schott, Swallow, & Fieux, 1990; SM) as well as shedding outflow toward the east, proceeding just north of the equator where the Ekman transport is southward and will return part of this water across the equator (Fig. 1).

North of the Southern Gyre, the Great Whirl (GW) spins up after the full-blown development of the SW monsoon. The upwelling occurring along its northern side recirculates cyclonically around the GW with very little eastward exchange in the 5–12° latitude band (e.g. Schott, Fischer, Garternicht, & Quadfasel, 1997) and partially exits northwards through the Socotra Passage east of the Horn of Africa as shown schematically in Fig. 1. A different and somewhat weaker upwelling regime with typically several filaments exists off the Arabian peninsula during the summer monsoon. Even weaker upwelling occurs off the west and east Indian coasts during the summer monsoon. There are, however, cyclonic circulation cells located both west and east of southern India and Sri Lanka (Fig. 1) for which models suggest a contribution of open-ocean upwelling.

During the winter monsoon, the flow south of about 10°S remains fairly unchanged against the above described summer monsoon circulation, but north of this latitude significant changes occur (Fig. 2). The upper-layer flow of the Somali Current is southward during winter monsoon, meeting the EACC at 2–4°S,

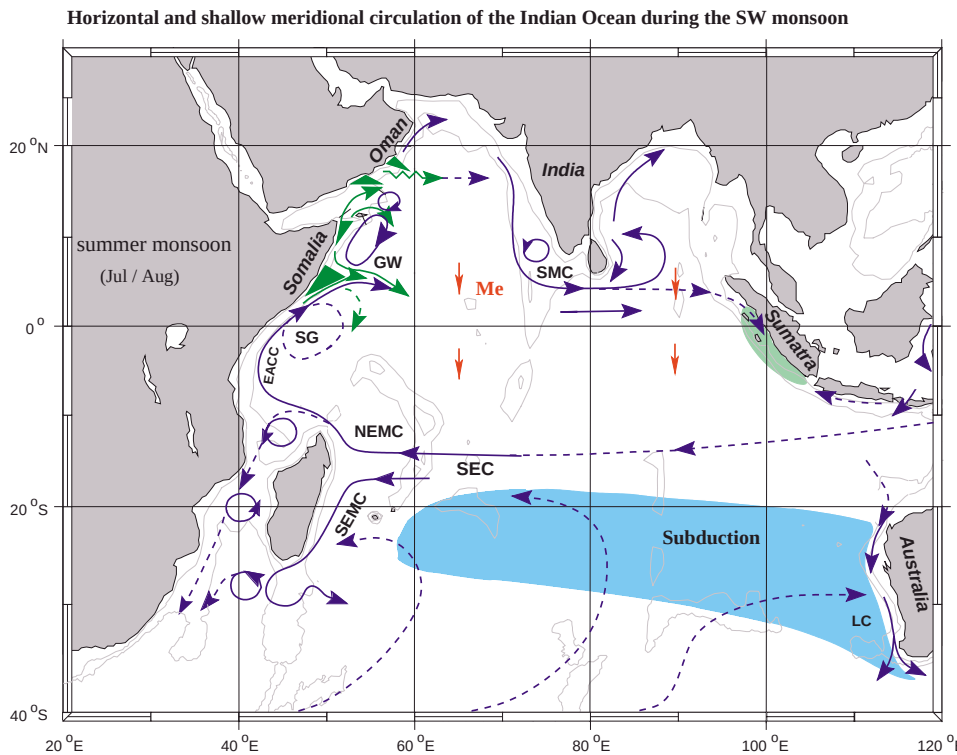

Fig. 1. A schematic representation of identified current branches during the Southwest Monsoon. Marked are winter subduction area in southern subtropics, approximately for densities in σ_θ=24.0–26.5 kg m^{-3} range (blue), upwelling areas (green) and southward Ekman transport on both sides of the equator (red). Current branches indicated (see also Fig. 2) are the South Equatorial Current (SEC), Northeast and Southeast Madagascar Current (NEMC and SEMC), East African Coast Current (EACC), Somali Current (SC), Southern Gyre (SG) and Great Whirl (GW), Southwest Monsoon Current (SMC), and Leeuwin Current (LC). (Modified from Schott & McCreary, 2001).

forming a confluence to supply the South Equatorial Countercurrent (Düing & Schott, 1978), while beneath the surface, northward flow across the equator continues in a Somali Undercurrent (SM).

Some subduction also takes place in the Arabian Sea during the winter monsoon (marked in Fig. 2) that will also contribute to supplying the upwelling zones. The major subduction product here is Arabian Sea surface water that gets both cooled and augmented in salinity, by cold and dry winter monsoon winds (Morrison, 1997; Schott & Fischer, 2000). Small quantities are also introduced into the upper and middle thermocline by the Red Sea and Persian Gulf outflows. For the shallow thermohaline cell discussed in this paper the different seasonal effects will have to be put together for an annual mean.

The waters upwelled during the summer monsoon off Somalia and Arabia can slowly propagate across the Arabian Sea (Fig. 1) and be transported southwards by the interior Ekman circulation (Chereskin, Wilson, Bryden, Field, & Morrison, 1997). What happens as the Ekman flow approaches the equator? Model analysis first suggested the existence of an equatorial meridional roll embedded in the upper-layer equatorial flow (Wacongne & Pacanowski, 1996). It is caused by the fact that while in the summer monsoon the Ekman transport on both sides of the equator is southward, the winds on the equator itself and consequently the meridional currents on the equator are northward. As first demonstrated by Philander and Pacanowski (1981), under these circumstances cross-equatorial surface flow develops in the direction of the wind, upwelling on the upwind side, and downwelling on the downwind side. A meridional pressure

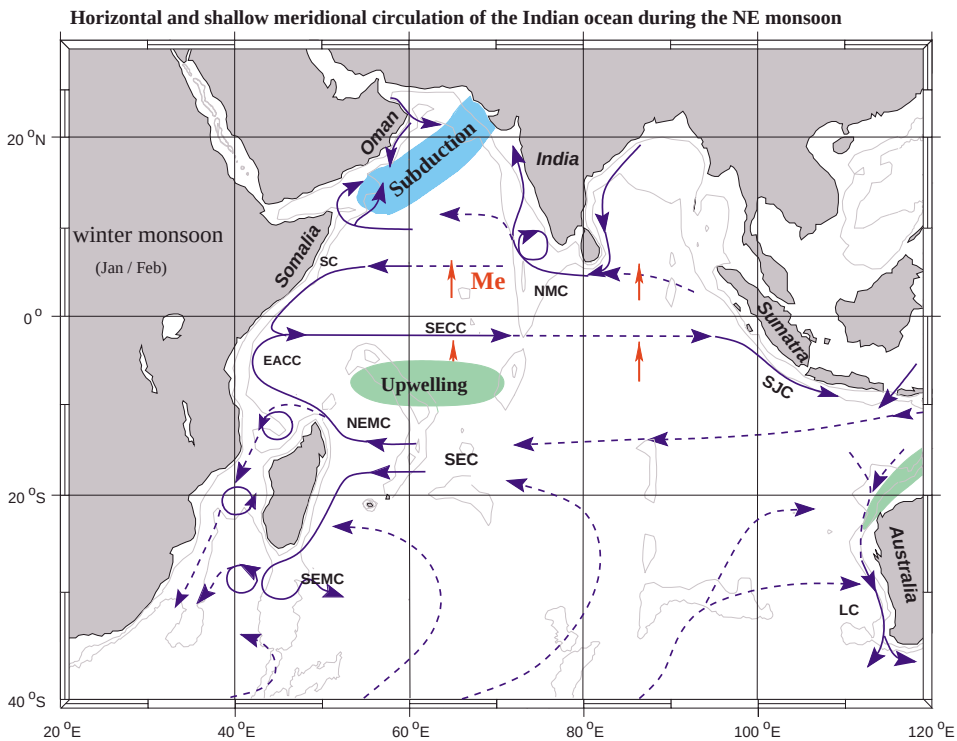

Fig. 2. As in Fig. 1, but for the Northeast Monsoon. Marked are the winter subduction area in the northern Arabian Sea (blue), upwelling off NW Australian shelf (light green) and presumed upwelling area in 5–10°S doming region, and northward Ekman transport on both sides of the equator (red). Current branches indicated are the South Equatorial Countercurrent (SECC), Somali Current (SC), Northeast Monsoon Current (NMC) and South Java Current (SJC).

gradient develops that tends to balance the surface wind, and it drives the subsurface counterflow. The net effect of the equatorial roll is to connect the southward upper-layer flow across the equator and thus close the shallow cross-equatorial cell. This equatorial roll is present in different recent high-resolution model evaluations of stream transport functions (e.g. Garternicht & Schott, 1997; Lee & Marotzke, 1998). For the particular meridional profile of the zonal-mean wind stress in the equatorial zone, which shows linear meridional shear across the equator, it has recently been demonstrated that the Ekman transport at the equator is finite and equals the Sverdrup transport (Godfrey et al., personal communication; SM).

During the winter monsoon, the situation is reversed: the Ekman transports are now northward on both sides of the equator (Fig. 2) and meridional wind components on the equator are southward, causing a roll with reversed circulation compared to the summer monsoon.

In this presentation we will discuss the observational evidence on the shallow thermohaline overturning circulation in the Indian Ocean. We will begin by reviewing the seasonal wind fields and resulting Ekman and Sverdrup transports. This analysis includes time periods associated with recently observed large equatorial anomalies (Saji, Goswami, Vinayachandran, & Yamagata, 1999; Xie, Annamalai, Schott, & McCreary, 2002; Yu & Rienecker, 1999) that for some time revert the eastern Indian Ocean to an upwelling regime. Next we look at the subduction in both the Southern Hemisphere and in the Arabian Sea. Then we discuss upwelling and related water mass transformations, and the sinking of the subducted waters. Besides concentrating on the effect of the major upwelling areas off the East African and Arabian coasts, we will also inspect other potential upwelling contributors in the interior subtropics and along at the eastern

margins, also in conjunction with the equatorial anomalies. Finally, a focus of the paper will be on the equatorial roll described above, based on observations made during WOCE, especially a moored ADCP array in the central Indian Ocean (Fig. 3), but also by re-assessing observational results from earlier publications. We close by summarizing the respective roles of the different discussed thermohaline circulation branches.

While focussing on the observational evidence, we will also relate our findings to results that we derived from the Simple Ocean Data Assimilation (SODA) of Carton, Chepurin, Cao, and Giese (2000), and refer to recent Indian Ocean model studies addressing the shallow cross-equatorial overturning circulation (Miyama, McCreary, Jensen, & Loschnigg, 2002; Godfrey et al., personal communication).

2. Atmospheric forcing

2.1. Monsoon season mean stresses and Ekman transports

The wind-stress fields for January, April, July and October, respectively, from the NCEP seasonal-mean climatology from 1990–98, illustrate the drastic changes of the monsoon (Fig. 4). South of about 10°S, the SE Trades persist throughout the year. As discussed by SM, among others, the different available wind stress climatologies can yield fairly large differences, strongly affecting, for example, the resulting equatorial currents in model simulations. Since we will address the main features of the wind-stress fields in this section, which are present in all the climatologies, we shall not comment on these differences further.

The Trade winds attain their seasonal maximum and most northerly extent during southern winter. In the Northern Hemisphere the monsoon winds are directed away from the Asian continent during winter,

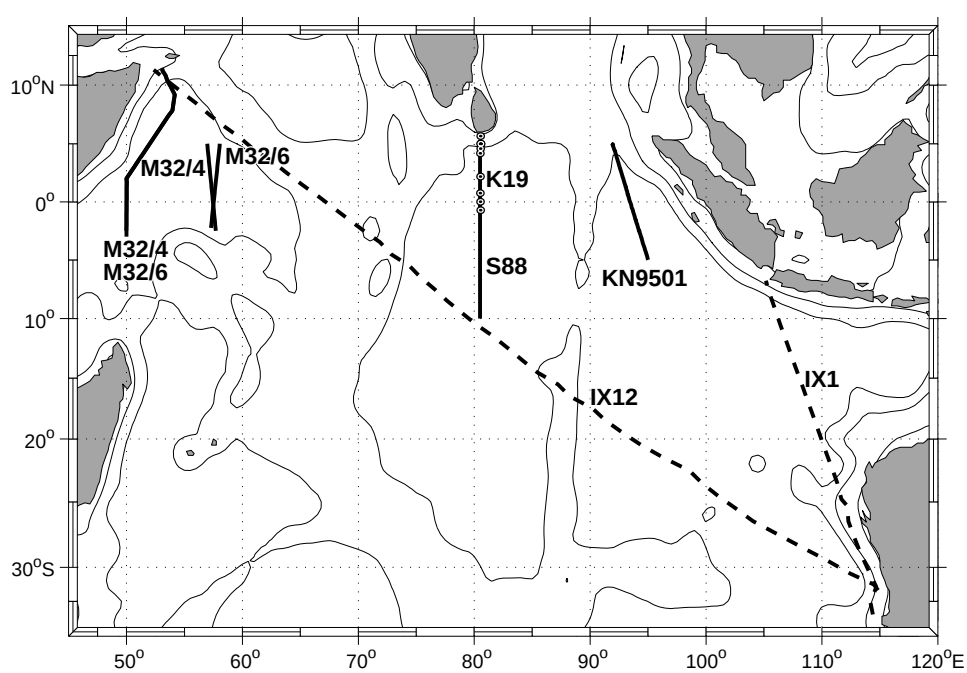

Fig. 3. Location of equatorial moored array at 80.5°E, of shipboard ADCP/CTD sections (solid) and XBT sections IX-01 and IX-.12 (dashed) referred to in this study.

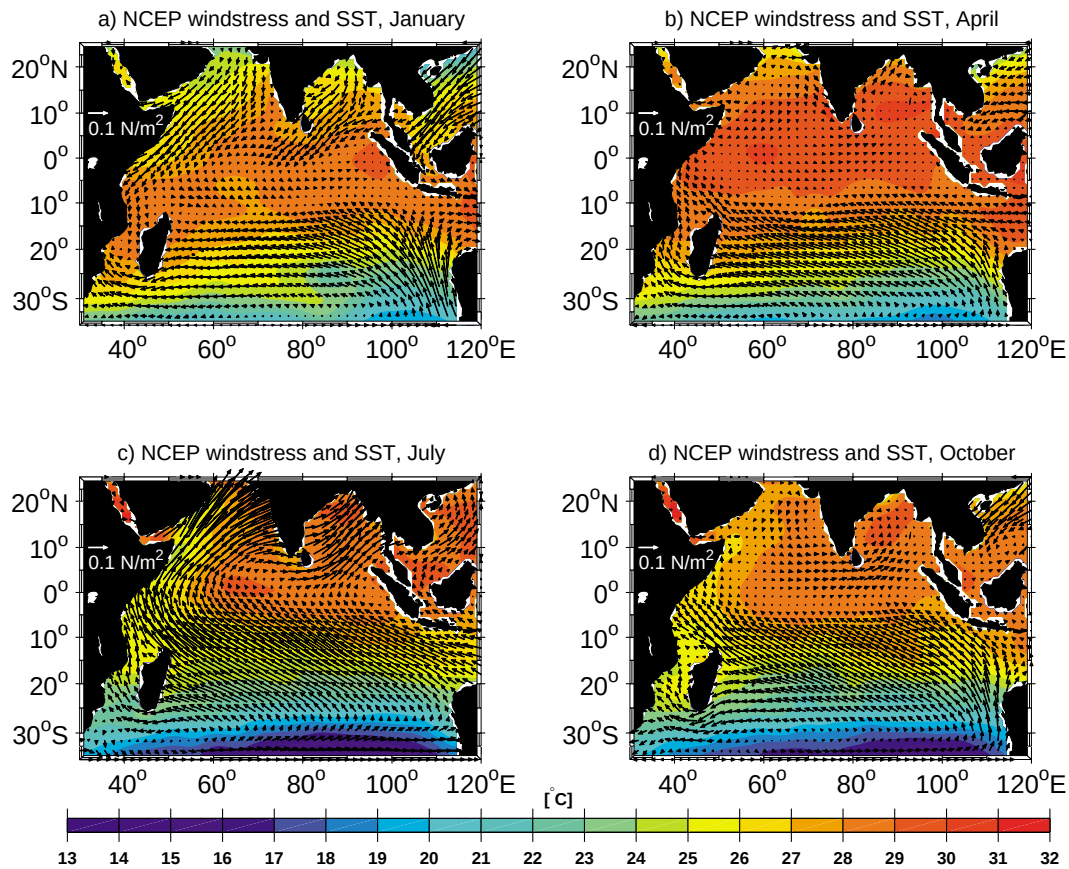

Fig. 4. Monsoon wind stress fields from the 1990–98 NCEP climatology for (a) January, (b) April, (c) July and (d) October; underlaid (see colour code) are surface temperatures from the Levitus and Boyer (1994b) climatology.

causing southwestward wind stresses over the Arabian Sea and Bay of Bengal (Fig. 4a). Whereas during the summer monsoon the stresses are northeastward over the northern Indian Ocean (Fig. 4c).

Over the western basin there is a continuation of the southern-hemisphere trade winds into the Arabian Sea during the summer monsoon, with strong northward cross-equatorial stresses, forming a narrow atmospheric jet. The SE Trades extend to near 5°S at this time. In the Arabian Sea Ekman convergence and mixed-layer warming occurs and there is Ekman divergence and cooling in the northwest (Figs. 4c and 5c). During the summer monsoon, wind stresses have an eastward zonal component north of the equator (Fig. 4c) and a westward component south of the equator in the Trades domain, i.e. they drive southward Ekman transports on both sides of the equator (Fig. 5c). The wind directly on the equator is northward during the summer monsoon, i.e. directed against the off-equatorial Ekman transports in both hemispheres (Fig. 4c). This meridional component is strongest in the west.

Between the monsoon seasons, i.e. April–June and October–December, wind stresses on the equator are eastward (Fig. 4b,d) so that on the equator there is convergence, rather than divergence as in the other oceans, leading to twice-annual eastward surface jets (Wyrtki, 1973).

During the winter monsoon, there is a belt of eastward wind stress between the equator and the Trades that are limited to the south of about 10°S. Ekman divergence and thermocline doming (Fig. 5c) at the northern edge of the Trades are largest at this time, as shown by the topography of the σ_θ =

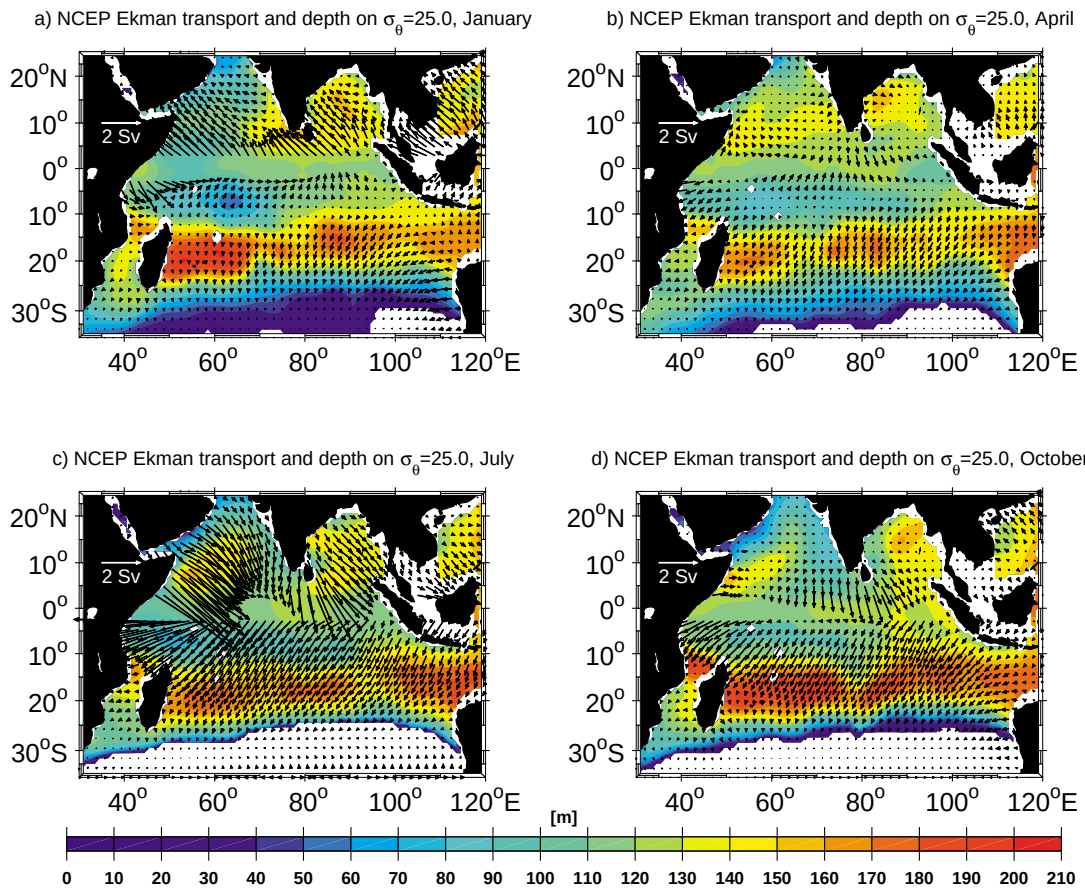

Fig. 5. Maps of Ekman transports for (a) January, (b) April, (c) July and (d) October from 1990–98 NCEP climatology; underlaid (see colour code) are depths of isopycnal $\sigma_\theta = 25.0$ kg m^{-3} from the Levitus and Boyer (1994a, 1994b) climatology.

25.0 kg m^{-3}. Regarding the zonal-mean stresses we have the opposite situation during the winter monsoon compared to the summer monsoon (Figs. 4a and 5a): north of the equator, wind stresses have a westward zonal component and south of the equator, an eastward zonal component. As a result Ekman transport is northwards on both sides of the equator during this season. And on the equator the meridional stress is southward during the winter monsoon, which is again against the Ekman transport.

In the annual-mean wind stress distribution, the summer monsoon pattern dominates with anticyclonic stresses over the Arabian Sea (Fig. 6a). Hence, the mean curl is negative north of 18°S, with the exception of some coastal regions. The resulting mean Sverdrup transport function (Fig. 6b) shows the observed subtropical and SEC circulation of the South Indian Ocean, a weak mean cell in the Somali current area and implies a mean southward transport of −6.5 Sv across the equator for the NCEP climatology, with a standard deviation of ±0.9 Sv of the annual-mean values for the time period 1990–98.

As Godfrey et al. (2001) and Miyama et al. (2002) pointed out, the zonal component of the winds nearly vanishes at the equator during both monsoons, and it is roughly proportional to the distance from the equator on either side. For this wind field they showed that the concept of Ekman flow is valid all the way to the equator. Since this special zonal wind drives no geostrophic currents, the cross-equatorial flow is equal to the Ekman drift. Consistent with this idea, the quasi-steady Sverdrup flow has southward, cross-

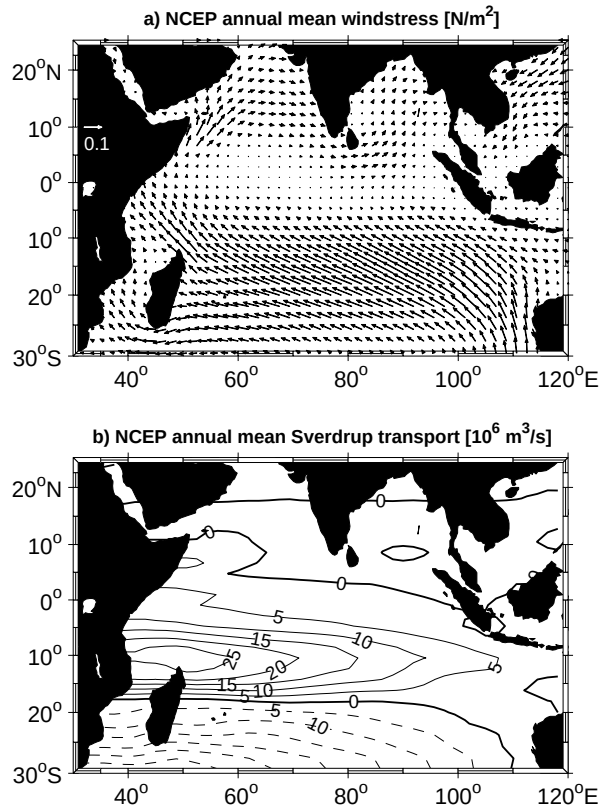

Fig. 6. Annual-mean fields of (a) wind stress, (b) Sverdrup transport function from 1990–98 NCEP climatology.

equatorial transports in excess of 30 Sv at the height of the summer monsoon and weaker, northward, cross-equatorial flow in winter (SM).

The Ekman annual-mean meridional Ekman transports (averaged for 1990–98) from NCEP across 3°N and 3°S are -6.9 ± 3.6 Sv and -6.0 ± 3.9 Sv, respectively, i.e. they agree with the cross-equatorial NCEP Sverdrup transport of -6.5 ± 0.9 Sv. The same averages for the ERS-1/2 scatterometer winds yield -7.4 ± 4.0 Sv across 3°N and -9.3 ± 6.4 Sv across 3°S with the Sverdrup transport across the equator at -6.4 ± 2.6 Sv. It is worth noting for the later model comparison, that the mean cross-equatorial Sverdrup transports for July are -30.7 ± 3.1 for the NCEP stresses and -32.5 ± 12.5 Sv for the ERS-1/2 stresses. For January the numbers are 19.4 ± 2.5 Sv for NCEP and 21.5 ± 7.6 Sv for ERS-1/2, respectively.

The consistency of the cross-equatorial annual-mean Sverdrup transports among the products is reassuring, in particular on the background of the huge annual cycles and large interannual anomalies and the differences between the individual time series of both data sets (see next section).

2.2. Equatorial divergence during climate anomalies

While under normal conditions the Ekman transports on both sides of the equator during the monsoons are unidirectional, there are rare occasions where a strong equatorial divergence can occur. Hence, under these circumstances the equatorial Indian Ocean has the appearance of the other large oceans.

Two such events have been reported in recent years, in 1993/94 (Reppin, Schott, Fischer, & Quadfasel, 1999; Vinayachandran, Saji, & Yamagata, 1999) and in 1997/98 (Murtugudde et al., 2000; Webster, Moore,

Loschnigg, & Leben, 1999; Yu & Rienecker, 1999). These events are characterized by anomalous westward winds along the equator and consequently upwelling and cold SST in the east, and by warm SST and downwelling in the west. Whether or not these events are offshoots of Pacific ENSOs (1997 was a strong, 1994 a weak ENSO event) or whether they are independent Indian Ocean Modes (Behera & Yamagata, 2001; Saji et al., 1999) is still a matter of debate (Xie et al., 2002).

Time series of the Ekman transport divergence anomalies across 3°N and 3°S and between Sri Lanka (80°E) and the eastern boundary, determined for NCEP (Fig. 7a) and for ERS-1/2 (Fig. 7b), respectively, show the magnitude of the 1994 and 1997 episodes. The mean cycles of both climatologies, while differing significantly, show the semiannual harmonic resulting from the spring and fall Ekman convergences (negative in Fig. 7a,b) and Wyrtki Jets. Divergences occur early in the year and again in July–August, generating the situation for the observed eastward equatorial undercurrents in boreal spring and again in summer (SM). The 1994 and 1997 Indian Ocean anomalies are coupled to the annual cycle with the maximum eastern thermocline shallowing occurring toward the end of the year (Webster et al., 1999; Xie et al., 2002). This can also be seen in Fig. 7c, which shows anomalies of SST and of the 20°C isotherm depth from off Sumatra, from the northern end of the XBT line IX-01 (Fig. 3).

Besides the anomalous eastern equatorial divergences observed during May to December 1994 and again during June 1997 to March 1998, there was also an anomalous divergence in 1991, an event not noted as an Indian Ocean Mode. This was a year where an ENSO event started to develop with the cloud fields over Indonesia beginning to move eastward and convection beginning to occur over East Africa, however conditions then reverted to normal (Murtagudde, personal communication, 2000), and thus effects similar to the other two events could not develop in the Indian Ocean.

The 1994 event was preceded by an anomalously strong fall WJ in 1993 (Reppin et al., 1999) as also seen here by the convergence, and similarly there was an anomalous convergence preceding the 1997 episode throughout the second half of 1996.

2.3. Surface density fluxes

Da Silva, Young, and Levitus (1994) determined density fluxes from the Comprehensive Ocean–Atmosphere data set (COADS) and found that integrating heat fluxes over all oceans resulted in a global net heat gain of 30 W m^{-2}; consequently they supplied a ‘constrained’ climatology in which this value is subtracted everywhere. A more recent evaluation using the SOC climatology of the Southampton Oceanography Center (Josey, Kent, & Taylor, 1999) yields heat fluxes that basically agree within about 10 W m^{-2} with the ‘unconstrained’ results of da Silva et al. (1994) for the Indian Ocean.

The density flux distributions into and out of the ocean derived from the ‘unconstrained’ da Silva heat and freshwater fluxes for the annual mean distributions (Fig. 8a) show positive density fluxes, i.e. into the ocean, in the 15–45°S latitude belt. There are two regional extrema in the Southern Hemisphere. One is located over the eastern subtropical gyre and is caused by a combination of high evaporation minus precipitation and cooling. This is the region of Indian Central Water formation. The second region is in the southwest, where the warm Agulhas Current water masses, after flowing down the African coast and in part returning eastward within the Agulhas retroflection, become exposed to colder air masses. Here, in the region where Subtropical and Subantarctic Mode Water forms (McCartney, 1982), the influence is predominantly thermal. The annual average shows that the northern Indian Ocean is losing density at the surface, because of the overwhelming influence of the summer monsoon (Fig. 8b), whereas in winter there is positive density flux in the northern Arabian Sea (Fig. 8c), i.e. subduction can also occur there.

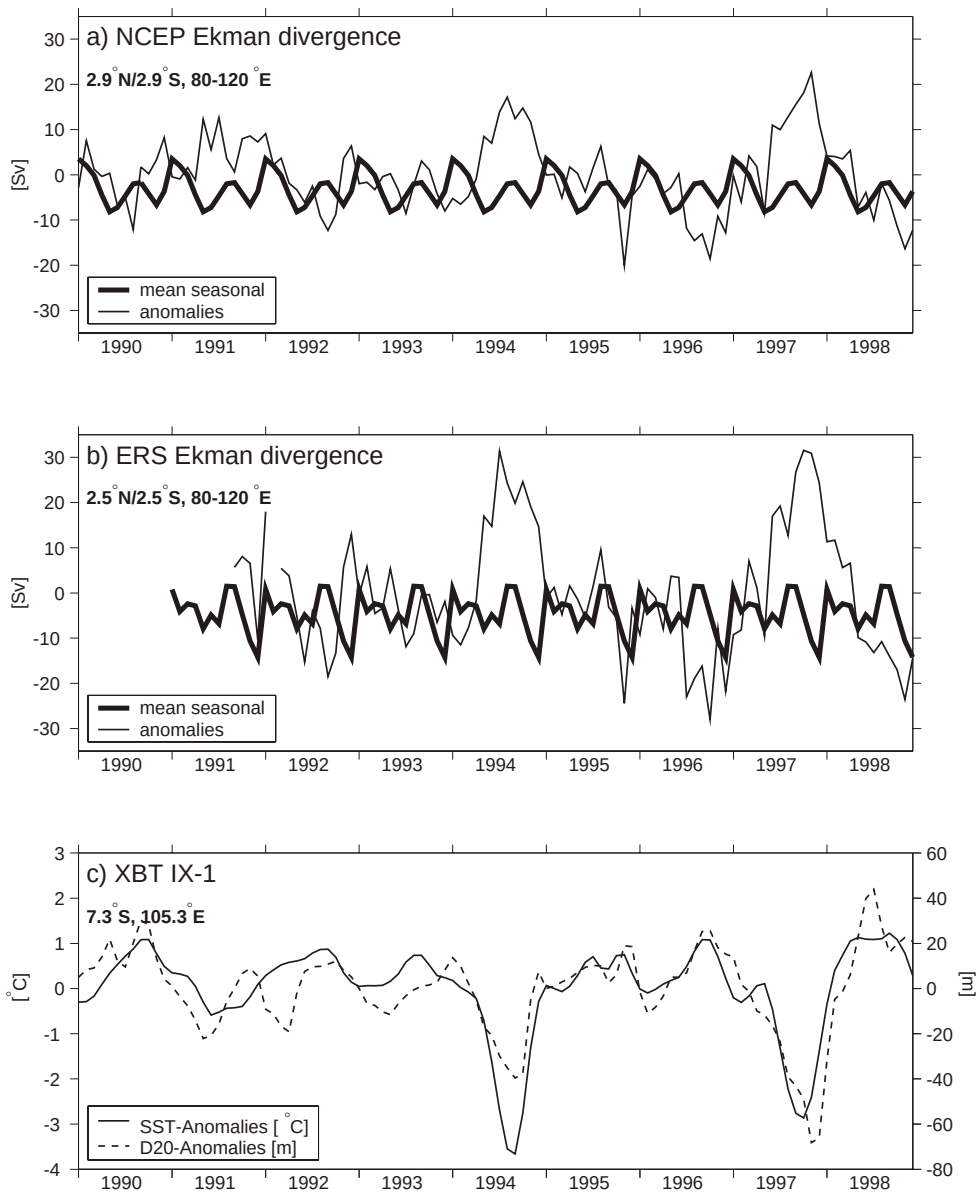

Fig. 7. Time series of equatorial Ekman transport divergence (positive) and convergence between 3°N and 3°S, and between 80°E and eastern boundary for 1990–98, based on monthly-mean stresses of (a) NCEP, and (b) ERS-1/2 scatterometry. Heavy curves are mean seasonal cycles, light curves are anomalies. Note divergence anomalies of 1994 and 1997/98 (and also 1991). Also shown, (c), are anomalies of sea surface temperature and 20 °C isotherm depth off Sumatra, at northern end of IX-01 XBT line (Fig. 3).

3. Distributions on isopycnal surfaces and water mass pathways

As stated in Section 1, the upwelling that is necessary to close the shallow thermohaline cell does not occur along the equator in the Indian Ocean but occurs predominantly through coastal upwelling in the Northern Hemisphere. On the other hand, subduction predominantly occurs in the Southern Hemisphere.

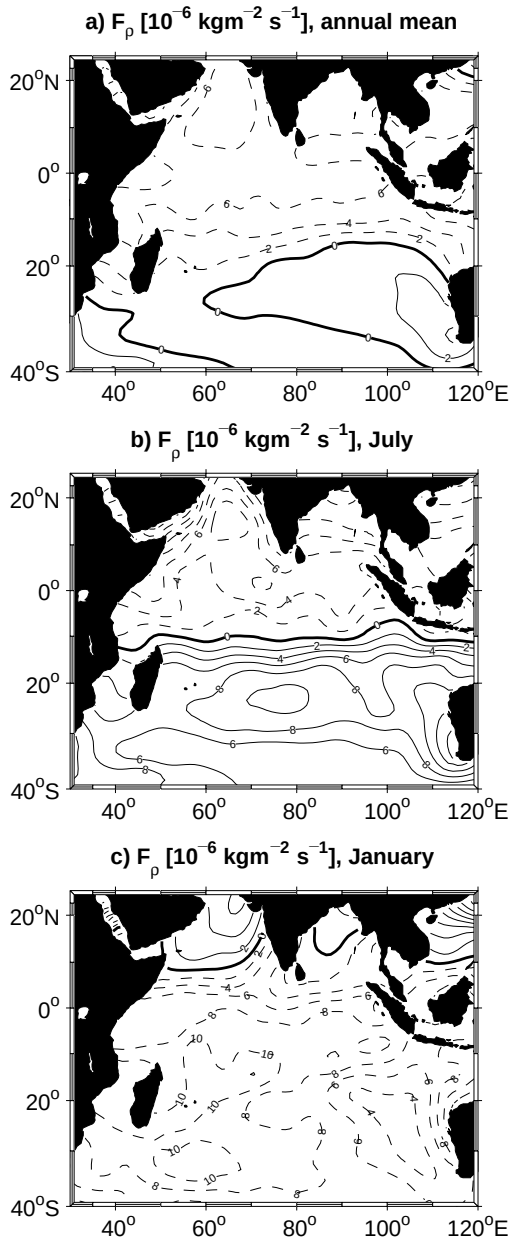

Fig. 8. Air–sea density flux (10^{-8} kg m^{-3} s^{-1}) positive into the ocean, (a) annual means, (b) January and (c) July for da Silva et al. (1994) climatology.

Hence, the shallow meridional cell must involve cross-equatorial flow. Water as dense as σ_θ = 26.5 kg m^{-3}, corresponding to temperatures of <16 °C, was observed during the early measurements of a very strong upwelling episode (Swallow & Bruce, 1966) off northern Somalia. However, during the WOCE sections observed in 1993–96 observed upwelling temperatures were more moderate, in the range

of 19–23 °C (Fig. 9a), which corresponded to densities in the range σ_θ=23.5–24.5 kg m^{-3} (Fig. 9c). But one has to bear in mind that during these later surveys, political constraints meant it was impossible directly to observe the upwelling regions inshore, so measurements of the flows could only be achieved further offshore (Fig. 3). As recently pointed out by Vecchi (personal communication), upwelling temperatures

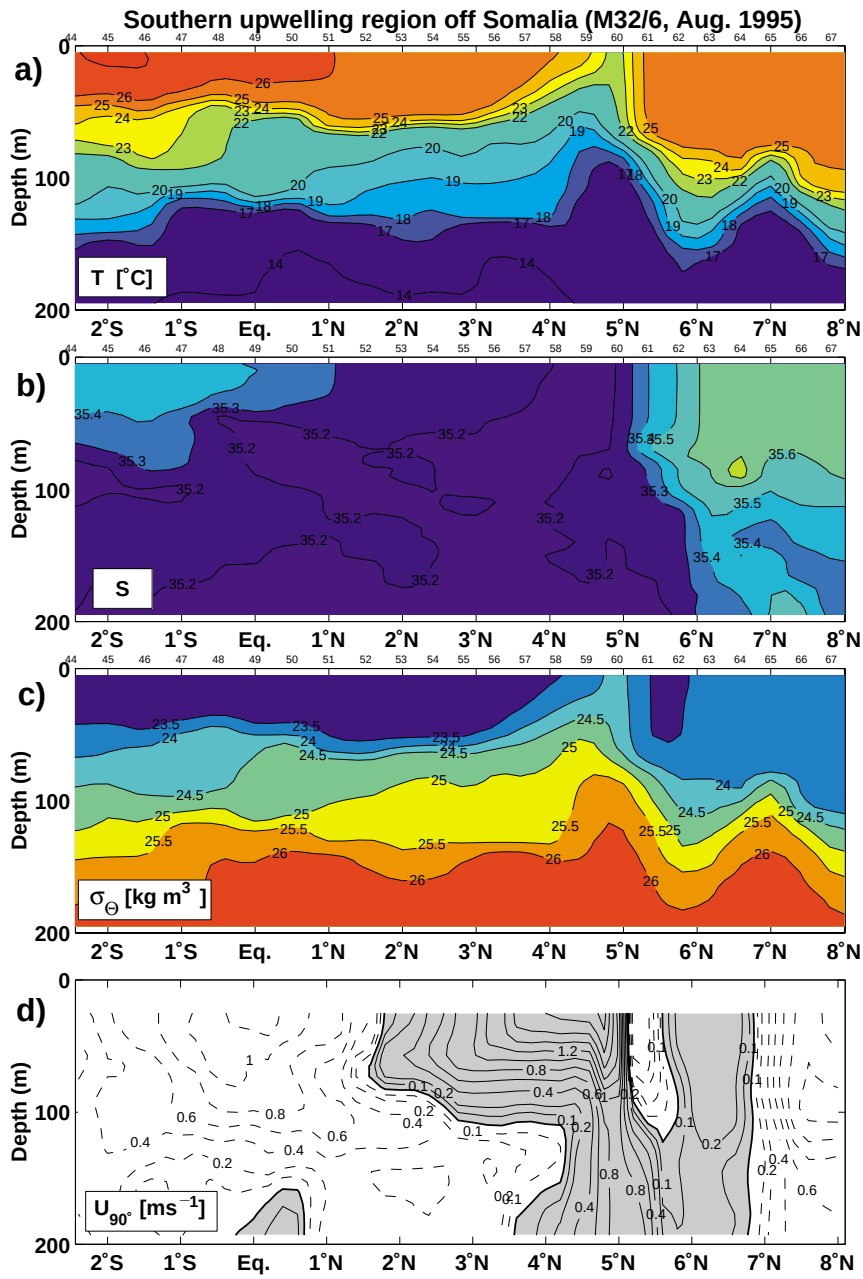

Fig. 9. Coast parallel section, taken on *Meteor* cruise M32/6 in August 1995 and running from equator to 6°N along Somali coast at offshore distance of 200 km (location see Fig. 3), (a) potential temperature, (b) salinity, (c) potential density and (d) ADCP current velocity normal to section for depth range 0–300 m.

off Somalia obtained by satellite AVHRR measurements are sometimes biased to higher values because of the effects of the cloud cover. Cloud presence results in low apparent satellite sea surface temperatures for a pixel, and the analysis routines, as also confirmed by R. Evans (RSMAS/U. Miami, personal communication, 2001), will insert climatological values if they encounter values considered too low for the region. Since clouds occur frequently over the Somali upwelling regions during the summer monsoon, the overall impression of the past decades maybe that the upwelled waters are warmer than they actually are. Hence, the Swallow and Bruce (1966) report may not be so unusual, after all. This is supported by the numerical model evaluation of Miyama et al. (2002), who tracked upwelling model particles back to their source regions and found that some of them crossed the equator in the Somali Current deeper than 300 m.

There is also upwelling along the low-latitude eastern boundary, off Sumatra (Fig. 1) during the summer monsoon and fall transition, when winds blow northwestward parallel to the coast and Ekman transports are directed offshore (Figs. 4 and 5, c and d). Off Sumatra, the densest surface water occurs in September at 23.1 kg m^{-3}, and during the dipole episode of 1997, the maximum of 23.5 kg m^{-3} was determined from the observations along the northern end of XBT line IX-01 (Fig. 3). A potentially important upwelling region may also be in the open ocean at 5–10°S and in some other regions, as will be discussed later, but all upwelling densities are less than $\sigma_\theta = 26.5$ kg m^{-3}.

Several authors have analysed the thermocline water mass distributions and circulation of the Indian Ocean (Karstensen & Quadfasel, 2002; McCarthy & Talley, 1999; You & Tomczak, 1993) and discussed the associated subduction, which dominantly occurs in the Southern Hemisphere. On a smaller scale, subduction also occurs under the northeast monsoon winds in the northern Arabian Sea during boreal winter. Surface to subsurface water mass conversion further takes place in the Red Sea and Persian Gulf. Here we limit our discussion to those water masses that affect isopycnals, which can at times interact with the surface somewhere in the Indian Ocean, i.e. above $\sigma_\theta \sim 26.5$ kg m^{-3}.

3.1. Subtropical to tropical water mass distributions

Thermocline waters from the Southern Hemisphere supplying the Arabian Sea upwelling areas have to cross the equator in the western boundary current. The reason is that meridional currents cannot cross the equator freely in the interior because the flow has to reverse the sign of its potential vorticity when changing hemispheres. In the western boundary current however, frictional effects can compensate the vorticity change.

Southern winter surface densities in the southern Indian Ocean within the density range 23.5–26.5 kg m^{-3} that can upwell off Somalia occur in latitude range 20–35°S (Fig. 10b). Waters subducted in this region would be carried westward with the SEC (Fig. 1). The latitude where the SEC east of Madagascar splits into a northward and a southward flowing branch is about 17°S (Swallow et al., 1988). However, water originating from further south can still make it to northern Madagascar with the northward geostrophic flow of the interior (e.g. Stramma & Lutjeharms, 1997). In the northern Arabian Sea, surface densities in January are 23.8–24.8 kg m^{-3} (Fig. 10a), i.e. water subducted there could also resurface in the Arabian Sea upwelling areas.

The two density surfaces in Fig. 11, shown here for the austral winter situation, represent the shallow and the deep part of isopycnals surfacing in the Arabian Sea upwelling regions. The surface $\sigma_\theta = 24.0$ (Fig. 11a) has a depth of 60–100 m in the southern subtropics. Temperatures on it are 23–24 °C in the SEC and off east Africa. In the summer monsoon it surfaces at the left side of the SW monsoon wind axis (Figs. 4c and 11a). The salinity on this surface in the Southern Hemisphere is marked by a minimum that spreads westward with the SEC at the Indonesian Throughflow latitude of ~15°S and then northward along the boundary with the EACC and Somali Current (Fig. 11a). The upwelling waters are, therefore, marked by having low salinity compared to the salinity-maximum waters of the Arabian Sea; temperatures in the Arabian Sea upwelling regions on this surface are 23–25 °C.

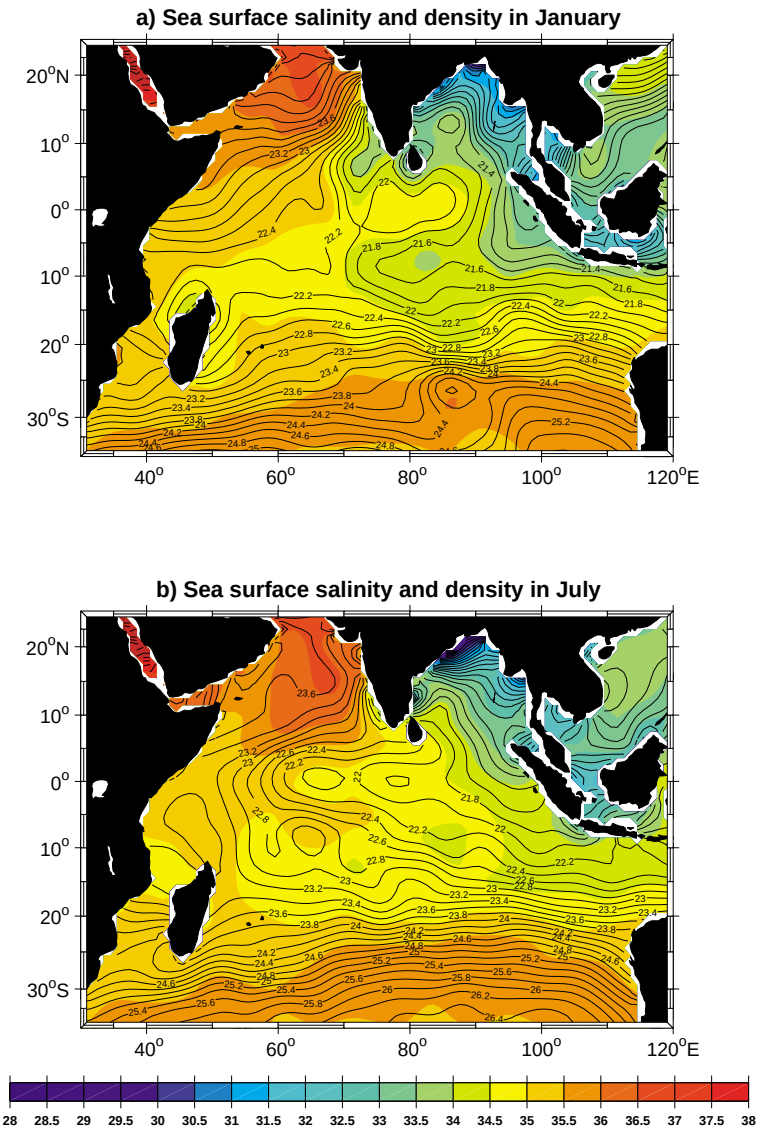

Fig. 10. Surface density (contours), underlaid by salinity (colours), (a) January and (b) July (from climatology of Levitus and Boyer, 1994a, 1994b)

The deeper range of the upwelling surfaces, which can come into contact with the atmosphere in the upwelling areas is represented by $\sigma_\theta = 25.7$ (Fig. 11b), which shoals from 240 m to 120 m as a result of the SEC in the 25–28°S latitude range and shows the deep Arabian Sea trough to the right of the wind axis typical for the SW monsoon. Temperatures on the 25.7 isopycnal are 17–18 °C, i.e. they correspond to the lower end of the range of surface temperatures observed off Somalia. Salinities again show the westward extending low-salinity wedge of the Indonesian Throughflow that passes north of Madagascar. Further, it shows higher-salinity waters from the southeastern subduction regions spreading northwestward with the SEC and lower salinities along the Somali coast than in the interior. Nutrient distributions on the

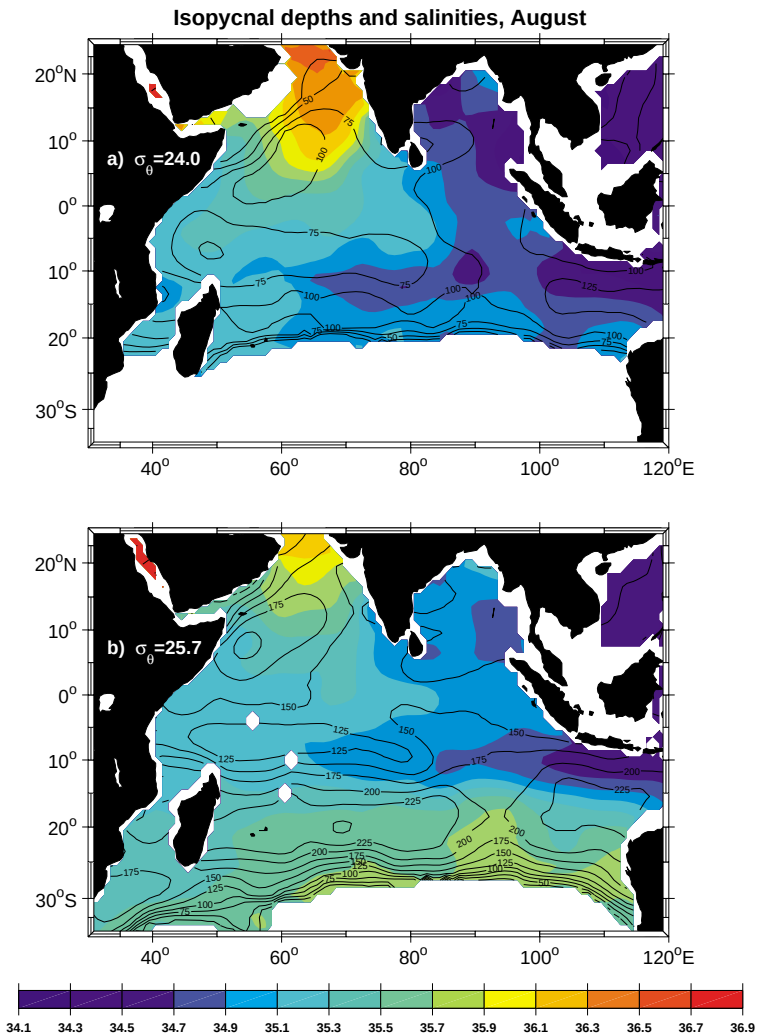

Fig. 11. Depths (contours) of and salinities (colours) on surfaces of potential density (a) 24.0 and (b) 25.7 kg m^{-3} for August.

σ_θ = 25.7 surface (Fig. 12) also show low values from the Southern Hemisphere spreading northward along the western boundary (You & Tomczak, 1993).

3.2. Western boundary circulation and pathways

The SEC supplies the NE Madagascar Current that in turn feeds into the East African Coast Current (EACC, Fig. 1). For the overall mean, about 30 Sv pass the northern tip of Madagascar above about 1000 m (Swallow et al., 1988), but of this only about 10 Sv crosses the equator with the Somali Current (Fig. 13c; Schott et al., 1990). While in the near-surface layer, above σ_θ = 26.5, Swallow, Schott, and Fieux (1991) found a continuation of the transports of about 17 Sv from North Madagascar over to the EACC, the thermocline layer, in the σ_θ=26.5–27.3 range, showed a flow deficit from the eastern to the western part of the northern entrance of the Mozambique Channel, that they estimated at 7 Sv, and suggested that this thermocline flow would pass southward through the Channel.

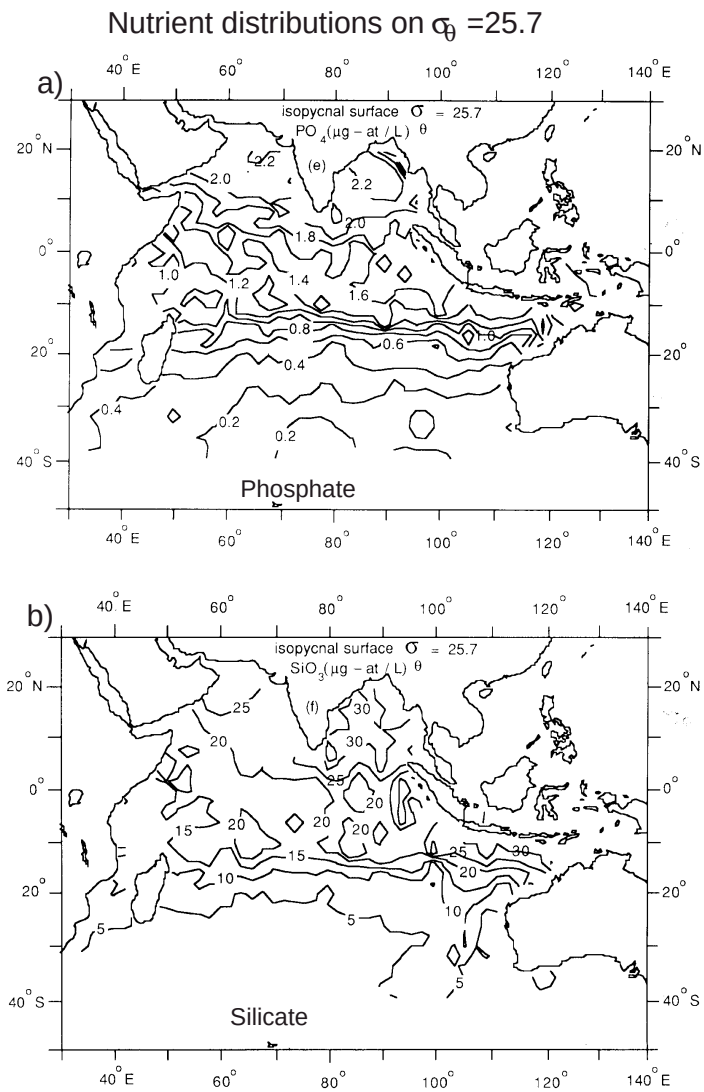

Fig. 12. Distributions of nutrients (a) PO_4 (μg–at/l) and (b) SiO_3 (μg–at/l) on the potential density surface $\sigma_\theta = 25.7$ kg m^{-3} (from You & Tomczak, 1993).

The continuation of the surface flow past the northern channel entrance is in agreement with surface drifter trajectories, for which we found (not shown) that out of 16 drifters arriving at the northern entrance only 2 passed southwards through the Channel. The majority followed the SECC flow toward the EACC and some that entered were trapped in eddies within the Channel. On the other hand, 5 out of 6 mid-depth (~1000m) float tracks shown by Di Marco et al. (2001) passed southwards through the Channel, confirming the deduction of a southward subsurface throughflow. A southward Mozambique Channel throughflow of 15 ± 9 Sv was determined in the global inverse model of Ganachaud, Wunsch, and Marotzke (2000). Overall, this combined evidence suggests that a significant fraction of the SEC waters arriving north of 17°S at the western boundary, and originates either as subduction within the Indian Ocean or is imported via the Indonesian Throughflow, does not participate in the Indian Ocean STC circulation but leaves south-

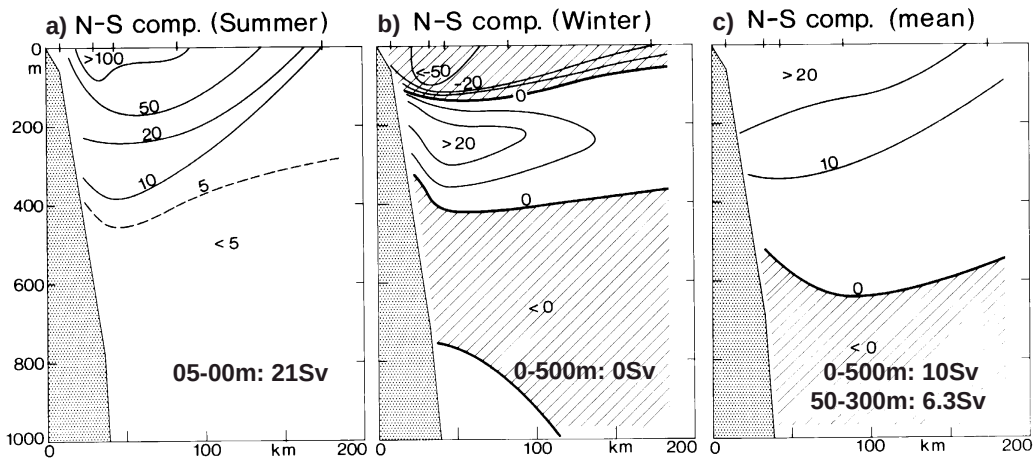

Fig. 13. Somali Current on the equator: cross-equatorial currents (northward is positive) during (a) the summer monsoon, (b) the winter monsoon and (c) for the annual mean (from Schott et al., 1990).

ward. These waters can then join the Agulhas and depart from there into the South Atlantic or become returned to the Indian Ocean via retroflection gyres. De Ruijter, Ridderinkhof, Lutjeharms, and Schouten (2002) suggest from T/P altimetry analysis that one of the mechanisms of Mozambique Channel throughflow could be by anticyclonic eddies (as sketched into Fig. 1) that are triggered at the northern end of the channel by Rossby waves arriving from the east. After passing through the channel these eddies presumably even affect the Agulhas retroflection and associated eddy shedding into the Atlantic.

Another fraction of the northern SEC/EACC inflow returns eastward just south of the equator during the winter monsoon with the South Equatorial Countercurrent (SECC, Fig. 2), as also derived in a recent geostrophic evaluation by Song and Gordon (2002).

As pointed out above, the subsurface cross-equatorial flow has to occur via the western boundary current, which was observed by Schott et al. (1990) with moored stations. They found that the annually reversing part of the Somali Current was restricted to not much deeper than the upper 100 m (Fig. 13a, b), with the stronger northward flow during the summer monsoon resulting in an annual northward mean of 3.5 Sv for the 0–100 m layer. Whereas below that, to a depth of about 400 m the flow was northward in both seasons, with large superimposed intra-seasonal variability. The transport in the 100–200 m layer was estimated at 2.7 Sv (using a combination of ship drifts and subsurface moored currents), with 1.9 and 1.1 Sv following below in the 200–300 m and 300–400 m slices, respectively. This would yield a total of 6.3 Sv for the 50–300 m layer supplying the upwelling density ranges. However, as pointed out by Godfrey et al. (personal communication), the deeper ranges of the northward flow, about 1.6 Sv in the 300–500 m range, must also participate in the upwelling, because dynamically they have no other way to go, since they cannot re-cross the equator southwards in the interior. In fact, model trajectories presented by Miyama et al. (2002) trace northern upwelling back to the cross-equatorial Somali Current at about 300 m depth.

One would expect that the errors on these layer means due to interannual variability of the particular (1984–86) monsoon seasons sampled as well as intra-seasonal variability and instrument coverage are not small. In the reversing surface layer, the standard deviations of the alongshore currents are larger than the means, in the 200–400 m layer they have the same magnitude as the means and below they are again larger than the means (Schott et al., 1990, their Table 2). Yet, for the 0–300 m range the difference between two independent annual means for different deployments was only about 20%, but for the weaker current regime below, it might well be that the northward mean flow does not extend much deeper than 300 m.

Besides the cross-equatorial cell there must also be southern hemispheric cells, relating subducted and Throughflow water masses with eastern boundary and open-ocean upwelling in the 5–12°S regime (e.g. Miyama et al., 2002), but these cells are not a focus of this paper

4. Estimates of subduction

4.1. In the Southern Hemisphere

Following Marshall, Nurser, and Williams (1993), the annual-mean subduction rate, S_{ann}, is determined as $S_{ann} = -(\mathbf{u}_m \cdot \nabla h_m + w_m)$ where the first term of the right hand side is the lateral induction term with $\mathbf{u}_m$ the horizontal velocity vector during late winter at the base of the winter maximum-depth mixed layer h_m. The effective vertical velocity w_m has to be determined from the annual-mean Ekman pumping velocity w_{ek} and a correction term which results from the vorticity balance constraint, i.e. $w_m = w_{ek} - (\beta/f)vh_m$, where v is the meridional velocity averaged over the mixed-layer depth.

Karstensen and Quadfasel (2002) calculated the Ekman pumping w_{ek} from the Hellermann and Rosenstein (1983) wind stress fields and used referenced geostrophic velocities based on the Levitus and Boyer (1994a, 1994b) data set. Different reference levels were tried out. They applied the method to the entire South Indian Ocean for densities in the range $\sigma_\theta = 23-27$ kg m^{-3}. In comparing the net pumping term w_m with the lateral induction term $\mathbf{u}_m \cdot \nabla h_m$ they found, as one might expect, that the induction term was large in the southern frontal zone.

The total amount of water subducted in this density range was determined at 34 Sv, with about half of this amount being contributed by the lateral induction term. Subduction in the density range <25.7 kg m^{-3} that has a depth of 150 m underneath the equatorial Somali Current (Fig. 11b) and can surface during strong upwelling cases amounted to 9.5 Sv, while a subduction rate of 3.0 Sv was determined for the density range $\sigma_\theta \leq 24.5$ kg m^{-3} that is typical for the weaker upwelling cases.

Errors on such numbers may result from inadequately sampled climatologies, as to be expected for the southern Indian Ocean, but also from decadal variability in the climatologies and resulting mismatches of the climatological 'means' of wind stresses and stratification. As an example, a repeat calculation by the authors using SOC 97 wind data instead of the HR winds amounted to a total subduction rate of 37 Sv. Furthermore, the effects of transient eddies, which were not included in the calculations of Karstensen and Quadfasel (2002), may also contribute to the subduction rate. The authors estimate the errors in their subduction volumes at 20–30% (J. Karstensen, personal communication, 2002).

The subducted water is transported westward with the SEC, along with Indonesian Throughflow watermasses; part crosses the equator northward and the other part returns southward on both sides of Madagascar as well as eastward with the SECC, as mentioned earlier.

4.2. Arabian Sea subduction during the NE monsoon

During the winter monsoon, the cold and dry Northeast Monsoon winds, combined with Ekman pumping, cause subduction of high-salinity surface waters in the interior northern Arabian Sea (Morrison, 1997; Schott & Fischer, 2000). This generates the widespread Arabian Sea Water salinity maximum just underneath the surface-mixed layer. The physical situation is favourable for subduction, because Ekman pumping occurs in the region of buoyancy loss (Fig. 8). Karstensen (personal communication, 2001) analysed the surface fluxes north of the equator during the winter monsoon and found that for the time period November–February density flux entered the ocean in the density range 23.3–25.0 kg m^{-3} at a rate of about 2–3 Sv, i.e. a rate corresponding to an annual rate of about 0.5–0.7 Sv. Ekman pumping is downward during the winter monsoon, and supports the occurrence of subduction. Boundary currents during the winter monsoon

are northward at the surface on both sides of Socotra (Fig. 2), but deeper down there are southward undercurrents (Schott & Fischer, 2000), which can carry subducted waters toward the upwelling regions of the next summer.

4.3. Exchange with northern marginal seas

Some conversion of surface to thermocline waters occurs within the Red Sea and Persian (or Arabian) Gulf. From moored array observations in the narrows north of Bab el Mandeb, Murray and Johns (1997) determined an annual-mean outflow of Red Sea Water of 0.3 Sv, with a seasonal cycle, ranging from 0.1 Sv in summer to 0.7 Sv in February. This water returns into the Indian Ocean through the passage between Socotra and the African continent and spreads at a core density of $\sigma_\theta = 27.2$ kg m^{-3}, below 600 m, i.e. it does interact with the upwelling. From the Persian Gulf the estimated outflow rate of Persian Gulf Water (PGW) is about 0.1 Sv (Koske, 1972) and this water spreads at $\sigma_\theta = 26.6$ kg m^{-3}, which is still below the upwelling depths.

In summary, a total of about 1 Sv of surface waters are annually transformed into subsurface waters north of the equator, in the open Arabian Sea and the northern marginal seas.

5. Estimates of upwelling

There are two main coastal upwelling regimes, off Somalia and off the Arabian peninsula. There is also weaker coastal upwelling during the SW monsoon off the west Indian coast and occasionally off the east Indian coast. The west Indian upwelling is weak, with SSTs of 26 °C in the upwelling zone, only about 2 °C colder than further offshore (Shetye et al., 1990). In the Southern Hemisphere upwelling is not observed along the western boundary. In the east, the Leeuwin Current is geostrophically driven against the prevailing (generally weak) northward winds, which can cause offshore Ekman transports at the period of their seasonal maximum which is November to March, but the upwelling effect is weak. There is, however, upwelling off Sumatra, in the Arafura Sea and along the NW Australian shelf. We will look at these different regimes in some detail in the following.

Furthermore, there are several regimes where open-ocean upwelling could presumably take place as a result of cyclonic wind stress curl and where numerical models yield upwelling transports, as reported later in the paper from the SODA model (Carton et al., 2000). One such region is at the northern edge of the Trades, at 5–10°S (Fig. 2) and then there are cyclonic circulation features on both sides of India during the summer monsoon (Fig. 1), the Sri Lanka Dome to the east (Vinayachandran & Yamagata, 1998) and the Laccadive Low to the west (Shankar & Shetye, 1997; Shankar, Vinayachandran, Unnikrishnan, & Shetye, 2002).

As mentioned earlier, this distribution of upwelling means that there must be other overturning cells besides the main cross-equatorial cell that connects the southern subduction regime and water masses stemming from the Indonesian Throughflow with the northern upwelling areas. In the Southern Hemisphere, the upwelling regimes off Australia, off Sumatra and in the 5–10°S belt must also be supplied by subduction and Throughflow which must involve separate local overturning cells in the southern hemisphere, as pointed out by Miyama et al. (2002).

5.1. Upwelling off Somalia

Upwelling off Somalia is associated with the development of the Somali Current gyres. It begins with the first northeastward alongshore winds in April–May, when the cross-equatorial flow turns offshore at 3–4°N, causing a noticeable cold wedge at its northern shoulder, and weaker upwelling to the north as a

result of offshore Ekman transports (Schott, 1983). With the onset of strong anticyclonic wind stress curl offshore in early to mid-June the Great Whirl is generated, with a second cold wedge at its northern offshore turning branch.

Somali upwelling during the fully developed monsoon thus is not by Ekman divergence spread out along the coast, but by the thermocline water being dynamically forced to surface to the left of the offshore flows, where mixed-layer processes and horizontal mixing by baroclinic instability can act to convert subsurface waters into surface waters. While the GW mostly recirculates to the south offshore (Fischer et al., 1996; SM), the Southern Gyre partially supplies a low-latitude eastward flow and partially recirculates across the equator (Fig. 1).

5.1.1. Outflow from the 'Southern Gyre'

In the coast-parallel section taken during *Meteor* cruise M32/6 in early September 1995, running 200 km offshore from the equator to 8°N (Fig. 3), the southern upwelling wedge can be identified by waters about 3 °C colder than its environment (Fig. 9a) and a salinity front separating southern ($S < 35.25$) from northern ($S > 35.45$) waters (Fig. 9b). The southern water turns offshore at speeds of up to 2.0 m s^{-1} while the northern water flows shoreward at >0.5 m s^{-1} (Fig. 9d). Fig. 14b,c show the detailed temperature–density and velocity structure near the front. Water of $\sigma_\theta < 24.5$ kg m^{-3} is in exchange with the surface near the front while away from the wedge the mixed-layer density is below 23.6 kg m^{-3}.

The question now is how to determine the fraction of the offshore flow that will not keep its thermocline properties but will either be exposed to surface heating and hence transformed into surface water or will be exchanged with warmer water by baroclinic instability. During the same cruise, a section box was completed, with the Southern Gyre in its southwestern corner (Fig. 14a). Temperature in the mixed layer (20–40 m) in the other parts of the sections are several degrees Celsius warmer than the offshore flow. Some recirculation of the dynamically lifted waters occurred, having densities larger than 24.5 kg m^{-3}. We make two kinds of estimates, high and adjusted. The high estimate assumes that the waters between σ_θ=23.5–24.5 kg m^{-3} that flow offshore at near-surface levels shallower than the typical wind-mixed layer depth of the region, which is about 50 m (Fig. 9), eventually lose their character as upwelled waters by radiative warming and cross-frontal mixing and so become transformed into surface waters (i.e. the area marked between both density contours in Fig. 14b). This assumption yields an upwelling rate of 8.7 Sv (Fig. 14c).

However, much of the water recirculates within the Southern Gyre, within a rather short time scale of a few weeks. With a net gain of about 70 W m^{-2} for the region (e.g. da Silva et al., 1994) a 50 m thick layer can only warm by about 1 °C over a time scale of a month. This warmer water will then re-enter the Somali Current at a slightly lower density level (i.e. shallower). It may then make more rounds through the gyre over the course of the monsoon, and rise further during each loop. Hence, a more conservative estimate would be to say that the core of the high-density outflow of Fig. 14 slumps back into the thermocline and that only waters in a density range within about 0.5 kg m^{-3} of the mixed-layer density will be transformed to upper-layer waters. The offshore transport within this density range amounts to 3.2 Sv (Fig. 14c), and we take this value as our adjusted estimate.

5.1.2. Outflow from the 'Great Whirl'

The water upwelled during the full-blown phase of the summer monsoon in the northern cold wedge at the offshore-turning flank of the 'Great Whirl' (GW) is partially carried into the Gulf of Aden by the northward throughflow that pases through the Socotra Passage between the island of Abd al Kuri and the African continent (Schott et al., 1997) and partially recirculates around the GW flow (Fig. 15a). From a ship section across the passage and moored time series within it (SM) the upper-layer northward outflow into the Gulf of Aden is determined at 2.1 Sv for the summer monsoon, as marked in Fig. 15a. As discussed in Schott et al. (1997) and SM, the water masses east of the GW have characteristics different from the

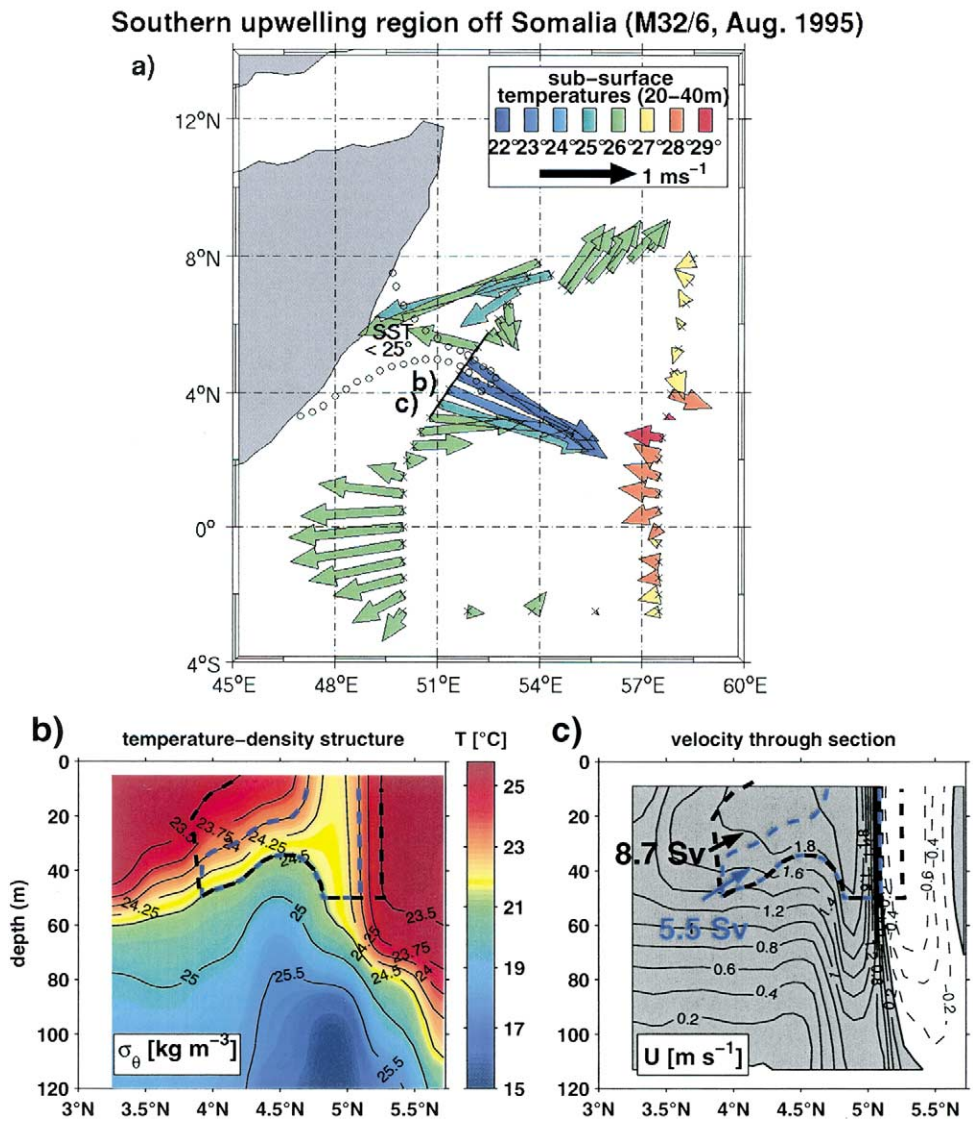

Fig. 14. 4. Upwelling and offshore flows out of the Southern Gyre near 4°N off Somalia for August 1995 (*Meteor* cruise M32/6): (a) near-surface current vectors between 2.5°S and 8°N with colours of temperatures at 20–40 m depth, dotted is satellite SST<25 °C line, (b) potential temperature (colours) and potential density (contours) across the offshore flow of upwelled water, marked is zone between σ_θ=23.5–24.5 kg m^{-3} and shallower than the general mixed-layer depth of 50 m outside the front, (c) currents and transports normal to section; transports are for total offshore flow within dashed boundary and for less dense outer margins only (blue, see text for details).

GW outflow. This is also evident from Fig. 15a, which shows a northward band of warm waters immediately east of the GW. The cold upwelled water is recirculated southward and returns into the GW at shallower densities after mixed-layer warming along the way. Exchange of GW waters with the interior thus occurs mostly through the Socotra Passage and by incremental warming within the recirculation.

The upwelled water has densities of 23.5–24.2 kg m^{-3}. Assuming again for the high estimate that all this water will be upwelled into the regional wind-mixed layer above 50 m and becomes permanently

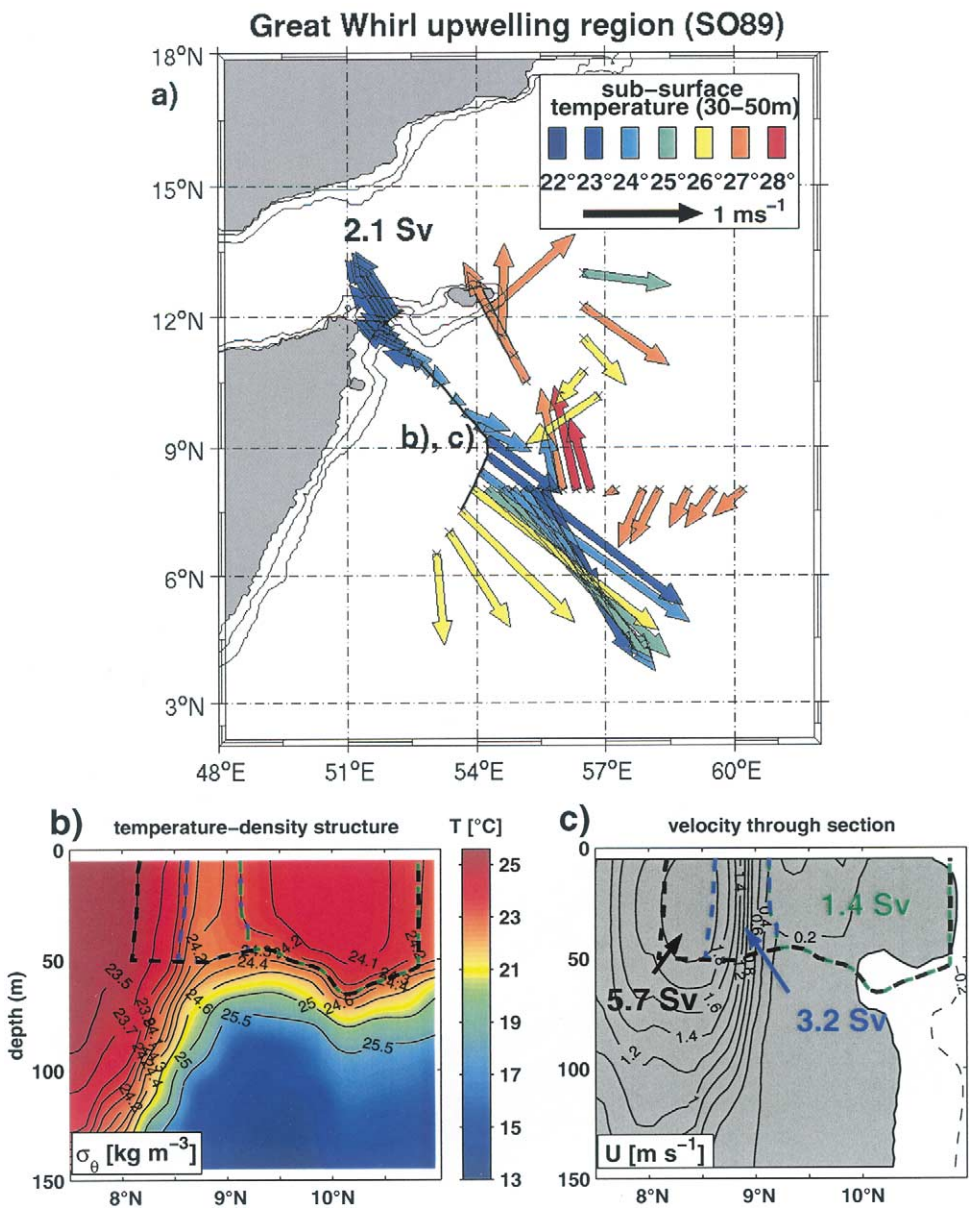

Fig. 15. Same as Fig. 14, but from Great Whirl and northern Somali Current, observed during *Sonne* cruise SO89 in August 1993: (a) outflows of cold upwelled waters are southeastward with the northern flank of the GW and northward through the Socotra Passage, (b) potential temperature (colours) and potential density (contours) density structure across northern GW flank, marked is zone between σ_θ=23.5–24.2 kg m^{-3}, (c) currents normal to section and transports through marked segment; transports are for the high-density core (blue) and the low-density northern and southern margins (see text for details).

transformed, yields an offshore upwelling transport of 10.3 Sv (marked section in Fig. 14b,c). For the lower adjusted estimate we assume that the fast-moving core of $\sigma_\theta > 24.0$ kg m^{-3} which transports 3.2 Sv, either slumps back into the thermocline or is recirculated within the GW; only two fractions of the outflow core are permanently transformed: the slow-moving part to the north of 9°N (1.4 Sv) and the waters in the density range 23.5–24.0 kg m^{-3} at the southern flank, above 50 m (5.7 Sv). This adjusted estimate yields an offshore upwelling transport of 7.1 Sv (Fig. 14c).

In summary then, the upwelling estimates from the southern Gyre plus the GW based on the 1993 and 1995 WOCE observations yield the following total: For the low (more realistic, we think) estimate the total is 3.2 Sv for the SG outflow, 2.1 Sv for the Socotra Passage outflow and 7.1 Sv for the GW outflow to the east, giving a total of 12.5 Sv. Taking this total as representative for a 4-month long monsoon period (June–September) would reduce this value to an annual total of 4.2 Sv. For the high estimate the addition of 8.7 Sv for the SG, 2.1 Sv for the Socotra Passage and 10.3 Sv for the GW yield a summer monsoon total of 21.1 Sv, corresponding to an annual mean of 7.0 Sv.

One also has to note here that our observations were taken 200 km away from the coast and some additional upwelling from deeper levels in that shore zone may have been occurring with subsequent water mass transformation before the eastward flow reached our offshore section. Just to give an example: if in a 500 km long by 100 km wide strip along the coast the upper 30 m of warm pre-monsoon mixed-layer water is replaced by upwelling water over a 3-months period that amounts to an additional upwelling rate of 1.2 Sv during the season, i.e. 0.4 Sv for the year, which is not totally negligible.

5.1.3. Comparison with offshore Ekman transport

The above-determined upwelling estimates from the focussed offshore flows can be put into perspective by comparison with the Ekman transports normal to the coast. The June–September mean offshore Ekman transport from the NCEP wind stresses (Figs. 4 and 5), determined for 1990–98 and between 2°N and 11°N, amounts to 19.5 ± 5.1 Sv, and for the ERS scatterometer wind stresses the corresponding mean summer monsoon offshore Ekman transport is 16.2 ± 4.0 Sv. These numbers support our high estimate more than the conservative one.

5.2. Off Oman

5.2.1. Coastal upwelling

Upwelling off southern Arabia occurs along the entire coast during the summer monsoon and the offshore flow is carried by filaments far into the interior Arabian Sea. The filaments develop in conjunction with mesoscale nearshore features and have a life time of a few weeks (Lee, Jones, Brink, & Fischer, 2000). The alongshore flow is eastward (Shi, Morrison, Böhm, & Manghnani, 2000), flowing past Ras al Hadd, the SE corner of Oman (Fig. 1) carrying the upwelled water into the warmer environment of the northeastern Arabian Sea (Böhm, Morrison, Manghnani, Kim, & Flagg, 1999).

Smith and Bottero (1977) made a first attempt at estimating the upwelling off Arabia, using geostrophic transports from ship sections normal to the coast between 52–60°E for the summer monsoon of 1963 and Ekman transports from ship winds. They estimated upwelling velocities close to the shelf in excess of 3×10^{-3} cm s^{-1} and an upwelling transport of about 2 Sv into the upper 50 m, which was compensated by onshore geostrophic flow in the 50–350 m depth range. Shi et al. (2000) analysed the upwelling off Oman for the summers of 1993–95 between Ras al Hadd and about 55°E, i.e. an alongshore extent of about 600 km. From a box budget calculation they estimated a summer monsoon mean upwelling of 2.2, 1.4, and 0.6 Sv, for the years of 1993–95 respectively, explaining the decrease with reduced offshore Ekman transports.

From a cold-water filament observed in August 1993 (Fig. 16a) we derived an estimate of offshore transports of upwelled waters on the same basis as discussed for Somali upwelling above. The mixed-layer

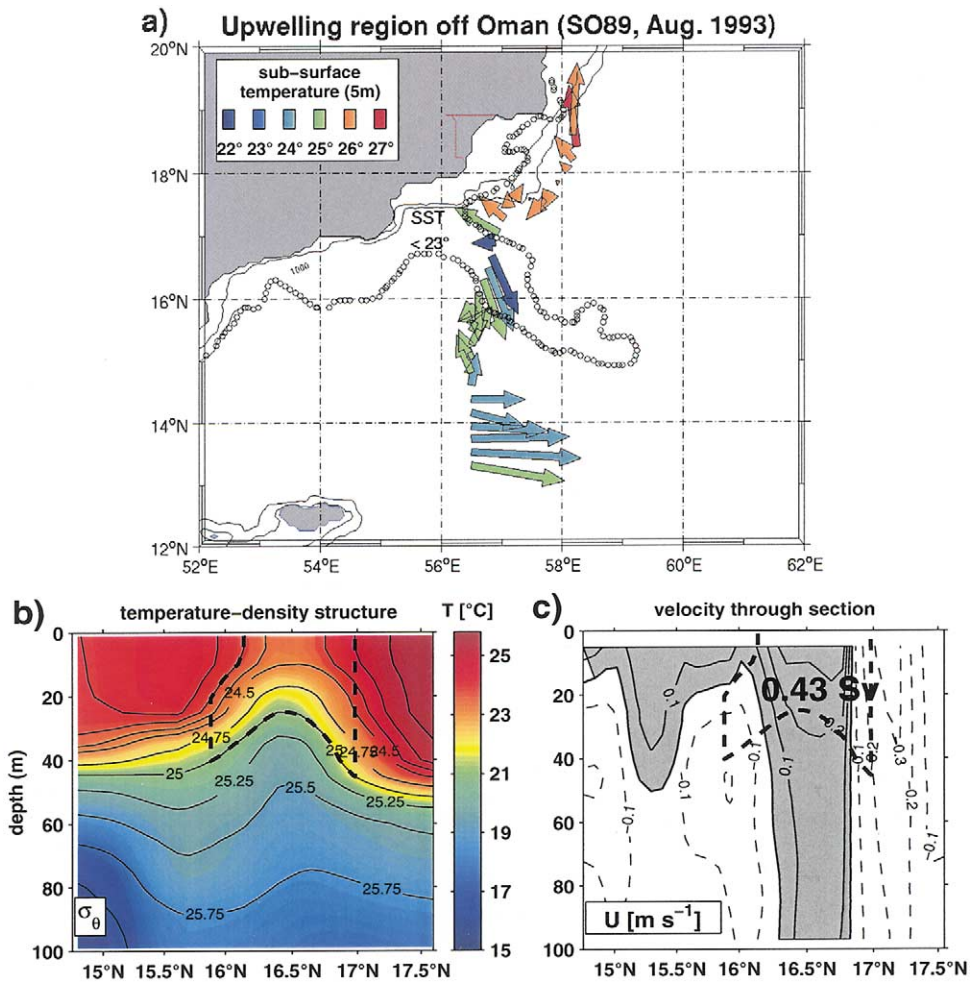

Fig. 16. Upwelling filament off Oman coast, observed during *Sonne* cruise SO89, August 1993: (a) near-surface ADCP currents and temperatures, dotted is satellite SST<23 °C line, (b) potential density across the offshore flow of upwelled water, marked is zone between σ_θ=24.3–24.5 kg m^{-3} and shallower than the general mixed-layer depth of 30 m, (c) currents normal to section and transport through marked segment.

in the region was only 20–30 m thick (Fig. 16b), and the filament transported waters in density range 24.3–24.5 with a total of only 0.4 Sv (Fig. 16). Another estimate for the effect of a filament like in Fig. 16a could be based on the fact that they are transient. Hence, if a filament area of 300 km by 100 km and 30 m thickness is assumed to be transformed by solar radiation from thermocline water to surface water within one month, this would yield an upwelling transport of 1 Sv, corresponding to 0.08 Sv annually.

Lee et al. (2000) studied Oman upwelling filaments by surveys of a towed undulating device, Seasoar, and obtained offshore transports of 1.6–5.8 Sv for upwelled waters at densities lighter than 25.0 kg m^{-3}; which has a depth of about 100 m off Oman. Scaling this with an estimated 2-week life-time of the filament, they arrived at an annual-mean upwelling transport rate of 0.06–0.23 Sv for the filament. This transport reaches fairly deep and recently, Fischer (personal communication, 2002) also determined transports of the filament above 24.5 kg m^{-3}, which has a depth of 40–60 m in the region and reported a reduction of about 25% of the above transport numbers, yet still significantly larger than what we observed earlier (Fig. 16).

Typically, about 3–4 filaments can be recognized off Arabia in remote sensing maps during the summer monsoon. Assuming that throughout the summer monsoon 3 filaments are at work for 3 months at a rate of 1.2–4.5 Sv above the density 24.5 kg m^{-3}, implies an annual mean offshore transport of 0.8–3.1 Sv by the filaments. In addition, upwelled water is transported eastward into the Gulf of Oman by the Ras al Hadd Jet. Out of the transport of 2–8 Sv for the summer monsoon reported for the upper 400 m of this current by Shi et al. (2000), corresponding to an annual transport of 0.7–2.7 Sv, only some fraction will become surface water.

The offshore Ekman transport off the Arabian peninsula between 14°N, 52°E and 22°N, 60°E, determined from the NCEP and ERS wind stresses for the time period 1990–98 and for the summer monsoon season, June–September, amounted to 3.0 ± 1.1 Sv and 3.1 ± 1.1 Sv, respectively. The corresponding annual mean is 1.0 Sv. That suggests that the appropriate choice for the total joint upwelling transports to deduce from above values may be more on the lower side of the observational range. We choose here a 1 Sv total as a reasonable annual average for the Arabian coast.

5.2.2. No offshore upwelling in the interior northern Arabian Sea

During the summer monsoon the Findlater Jet blows over the northern Arabian Sea, from Socotra to India, parallel to the Omani coast (Fig. 4c), causing enhanced entrainment and mixing along its path, Ekman pumping to the south and Ekman suction to the north (Fig. 5c). Weller, Baumgartner, Josey, Fischer, and Kindle (1998) analysed the mixed-layer deepening underneath a buoy located in the path of the Findlater Jet and measuring surface fluxes, and found that much of the mixed-layer variability there could be explained by local mixed-layer processes alone. Lee et al. (2000) compared the mixed-layer deepening of a Kraus–Turner model with the vertical velocities resulting from Ekman pumping for the northern Arabian Sea during the summer monsoon, using SOC wind stresses. They found that the local (Kraus–Turner) mixed-layer deepening on the northern (cyclonic) side dominates over the Ekman suction throughout the summer monsoon. Hence, open-ocean upwelling through Ekman pumping does not occur. Upwelled water found in the interior Arabian Sea has to be transported there by filaments and eddies out of coastal upwelling zones as described above.

5.3. Off India and Sri Lanka

Coastal upwelling off both sides of India has been described by Shetye et al. (1990, 1991). The upwelled waters off western India have densities of 23.5–24.0 but significant transformation into surface waters has not been documented. Upwelling off the east Indian coast is from much lower densities, σ_θ=21–22, than for the Arabian Sea (Shetye et al., 1991), and is also weak. This upwelling will, therefore, not be pursued further here.

However, numerical models of different physical complexity have yielded open-ocean upwelling both east and west of Indian and Sri Lanka (Miyama et al., 2002). In fact, when we calculate the Ekman divergence for a box 4–14°N, 72–85°E around southern India/Sri Lanka (same box boundary as in Miyama et al., 2002) and again subdivide it along 80°E, we obtain an annual-mean Ekman divergence of 1.4 (1.3) Sv from the NCEP (ERS-1/2) wind stresses for the western part and 2.8 (2.2) Sv for the eastern part. The stronger eastern divergence the result of the ‘Sri Lanka Dome’ described by Vinayachandran and Yamagata (1998), and the weaker western divergence results from the Laccadive Low during the SW monsoon (Shankar & Shetye, 1997). We will come back to that point later.

5.4. Southern Hemisphere

5.4.1. NW Australian shelf and Arafura Sea

The Ekman transports onto the NW Australian shelves were recently estimated by Godfrey and Mansbridge (2000) who found that maximum offshore Ekman transport over the NW shelf region, in

latitude range 10–24°S, occurred in austral summer, amounting to 2.5 Sv and that this offshore flow was compensated by geostrophic inflow above 200 m. By contrast, the Ekman transport out of the Arafura Sea, in latitude range 4–10°S, was found to attain its maximum of 1.2 Sv in July. In summary, both upwelling regimes can contribute about 1.4 Sv annually of offshore Ekman transport.

5.4.2. At the 5–10°S divergence

The Southeast Trades in the southern Indian Ocean terminate at a northern limit between 5–10°S (Fig. 4). This is associated with an Ekman divergence that is strongest during the summer monsoon (Fig. 5c) but is present year-round. In climatological maps of isotherm depths this region is marked by an uplifting of isotherms (Figs. 5 and 11). This zone shows a conspicuous upward transport in zonally integrated stream functions of several models (e.g. the evaluation of the Parallel Ocean Climate Model, POCM by Garternicht & Schott, 1997), suggesting that the dominant shallow thermohaline cell of the Indian Ocean might be the connection between subduction in the southern subtropics and upwelling at 5–10°S rather than involving a cross- equatorial STC branch by the Somali Current.

A section taken in July 1993 during *Sonne* cruise SO 88 (Fig. 17) and running from the tip of Sri Lanka at 6°N to 12°S shows an uplifting of the isotherms and isopycnals from about 100 m to near 40 m at 8°S. However, the upwelling is not detected in the surface temperatures (Fig. 17a) since it is a gradient region for mixed-layer temperature, which gets successively warmer as the section approaches the equator. Salinity on the other hand (Fig. 17b) shows a surface expression, but this is located north of the subsurface doming and is an unrelated feature. Inspection of XBT temperature sections of the WOCE IX-12 line (from http://www.marine.csiro.au) did indeed not show one section with a local SST minimum in that latitude belt. Nor is there a minimum in the mean climatological maps, e.g. Levitus and Boyer (1994a, 1994b).

On the other hand, support for this upwelling comes from satellite imagery of ocean colour, which sometimes indicates the presence of phytoplankton blooms along the band (Murtugudde et al., 1999) and also from nutrient distributions (Wyrtki, 1971). Other support for this upwelling comes from the correlation between thermocline depth and SST fluctuations, which shows a maximum in the 5–10°S latitude band as determined from the IX-12 XBT line (Fig. 3) data (Xie et al., 2002).

The potential relevance of STC interaction with the surface is due to by the fact that SSTs in this zone are near 28 °C (Fig. 18) and at this critical temperature even slight changes may have drastic impacts on the atmosphere, which might be much more severe than stronger SST changes off Somalia on a background of generally lower SSTs. High correlations of SST anomalies in this region with African rainfall anomalies (Reason & Mulenga, 1999) document this relevance.

Substantial upwelling in that latitude band is confirmed when evaluating Ekman transports. The Ekman divergence for the box 2–12°S, 50–90°E yields an annual mean of 8.6 Sv for the NCEP stresses (1990–98) and 9.8 Sv for the ERS-1/2 scatterometer stresses (1992–98).

5.5. In the eastern equatorial zone

Under normal conditions the equator is warm in the Indian Ocean, with winds even twice yearly blowing eastward, causing warm water convergence on the equator, in contrast to the situation in which westward winds generate Ekman divergence and cold water on the equator, as is typical for the other oceans. However, in recent years two occurrences of a striking equatorial anomaly have been observed, which have been identified as coupled climate modes (Murtugudde et al., 2000; Webster et al., 1999) and which transformed the Indian Ocean equatorial regime, at least in its eastern half, into an upwelling regime for a while; these have been termed the ‘dipole’ mode by Saji et al. (1999) and subsequently by others. In Fig. 7 we show the significant eastern Indian Ocean divergence resulting from these wind field anomalies. Yu and Rienecker (2000) reported from XBT ship section observations across the eastern cooling region that the equatorial thermocline had been uplifted during the 1997/8 episode by 70 m at the eastern end. The

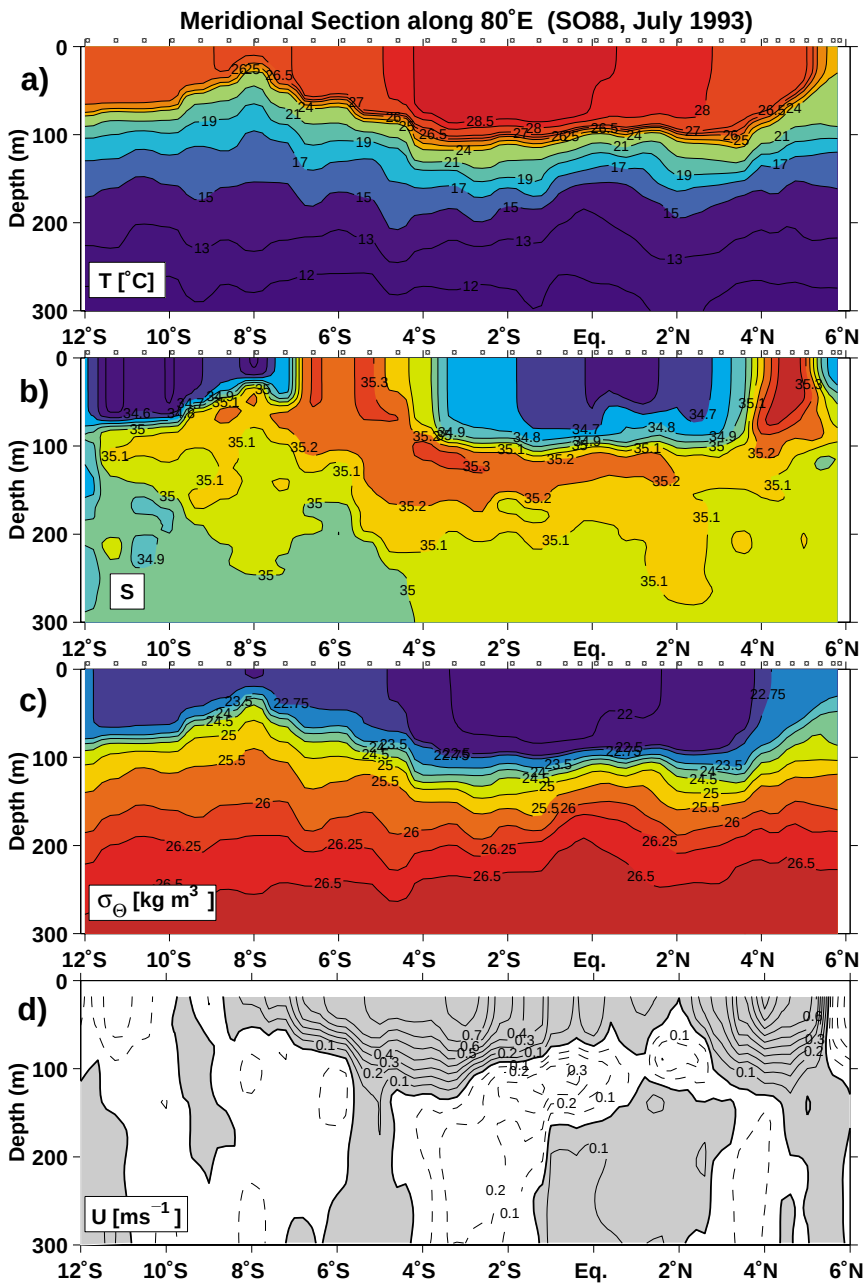

Fig. 17. Meridional section along 80°E (location see Fig. 3) taken during *Sonne* cruise SO 88 in July 1993: (a) potential temperature, (b) salinity, (c) potential density, (d) zonal currents.

20 °C isotherm depth anomalies off Sumatra from the northern end of the IX-01 XBT line (Fig. 7c) show that drastic shallowing during both episodes, 1994 and 1997. We evaluated the upwelling in the assimilation model of Carton et al. (2000) in this eastern equatorial zone and obtained about 20 Sv for boreal fall of 1997, in agreement with the Ekman divergences of Fig. 7. This transport is of course not equivalent to

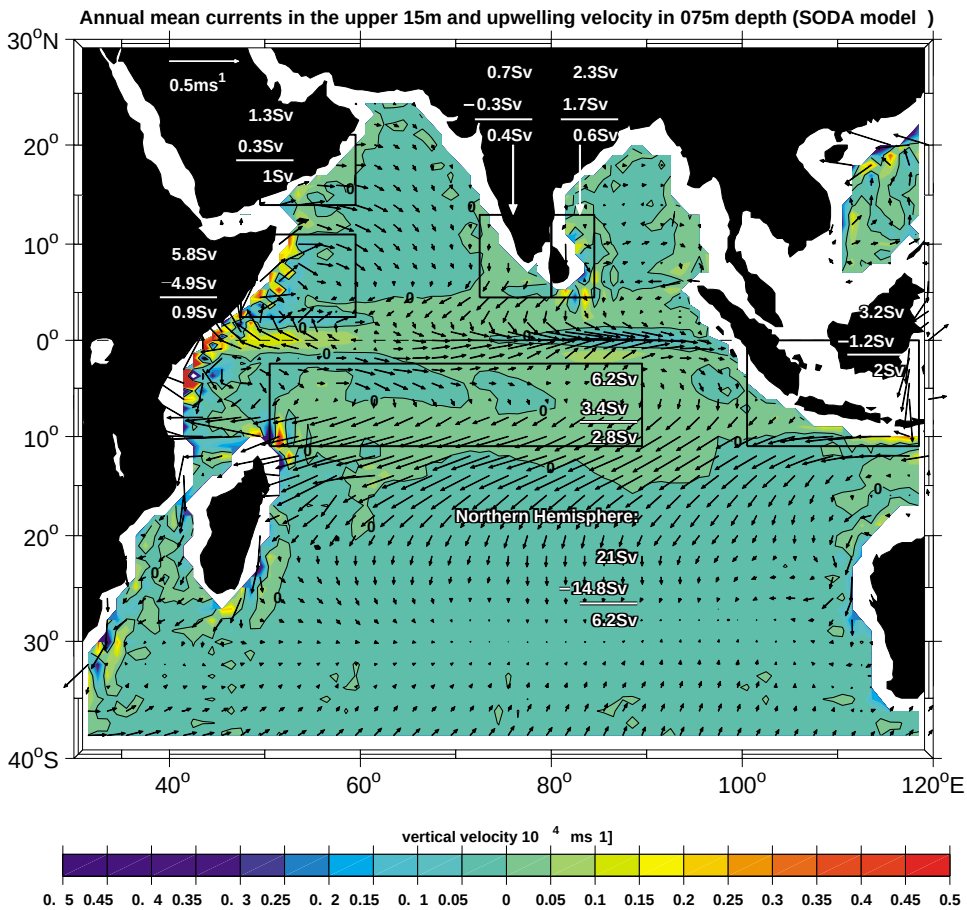

Fig. 18. Mean currents (upper 15 m, not every grid point shown; current scale see upper left) and vertical velocity at 75 m depth of SODA model. Shown for marked boxes are upwelling (positive), downwelling (negative) and net transports in Sv across 75 m level.

the amount of water mass transformation from thermocline to surface waters because the thermocline relaxes again at the end of the episode and the denser surface waters become thermocline waters again. The NCEP air–sea heat fluxes for the second half of 1997 yield near-zero net heat flux, with approximate cancellation of shortwave radiation gain and evaporative heat loss, which suggests that little density decrease of the upwelled waters during the anomaly episodes was possible. Nevertheless, some non-reversible upwelling had taken place, but it can be considered to be small compared to divergence numbers above and we have neglected it when estimating the overall mean.

As marked in Fig. 1, seasonal upwelling does occurs off Sumatra (Susanto & Gordon, 2001) in the late summer monsoon and fall but it is presumably weak and no estimates have been derived so far.

6. Upwelling and the cross-equatorial cell in the SODA model

Carton et al. (2000) used an ocean general circulation model to assimilate unevenly distributed ocean measurements (altimetry, surface temperatures, XBT tracklines, hydrographic stations, etc.) to produce dynamically consistent three-dimensional global fields of temperature, salinity and current velocity. This

Simple Ocean Data Assimilation (SODA) product is available at $1^\circ \times 1^\circ$ resolution in the mid-latitudes and $1^\circ \times 0.45^\circ$ longitude–latitude resolution in the tropics. There are 20 vertical levels with 15 m resolution near the sea surface. SODA thermocline variability of the Indian Ocean was evaluated by Xie et al. (2002) for the anomalies of 1970–1990 and it was found that the products looked physically reasonable in comparison with observations where available.

The mean circulation of the SODA model, as shown by the current vectors for the upper 15 m in Fig. 18, indicates the overwhelming effect of the summer monsoon, with northward Somali Current and anticyclonic circulation across the Arabian Sea. Upwelling (positive) and downwelling (negative) are marked for the same boxes in Fig. 18 as calculated by Miyama et al. (2002). The annual-mean upwelling across the 75 m level of the SODA model off Somalia is 5.8 Sv (somewhere between our low and high estimates), but that is nearly compensated by 4.9 Sv downwelling. If the same calculation as for Fig. 18 is done for the summer monsoon months only (not shown), a total upwelling of 15.3 Sv is obtained, reduced by 12.5 Sv downwelling to a net rate of only 2.8 Sv. The physics of the model upwelling process needs more exploration. One difference to the observations is that the SODA model does not reproduce the Great Whirl and Southern Gyre, the offshore flows of which are the basis of our upwelling calculations in Section 5.1; instead, the model upwelling occurs distributed along the coast. Furthermore, the vertical exchanges across a fixed level of this model type do not represent diapycnal upwelling rates. On the other hand, relatively weak net upwelling off Somalia was also obtained for layer models in the Miyama et al. (2002) study.

Total SODA upwelling off Oman is quite a bit smaller than off Somalia, only 1.3 Sv and there is a 0.3 Sv downwelling. Hence both the total and the net upwelling are in reasonable agreement with our mean estimate.

There are two regions where models suggest significant upwelling but observational evidence is difficult to obtain, around the southern tip of India and in the 5–10°S regime. Offshore from southern India and Sri Lanka, there is a total upwelling of 3.0 Sv (1.0 Sv net) in the SODA model (Fig. 18), mostly east of 80°E, i.e. in conjunction with the Ekman divergence associated with the Sri Lanka dome discussed in Section 5.3.

In the 3–12°S box the upwelling across 75 m in the SODA product was determined to be 6.2 Sv, as an average for 1990–99, but there was also downwelling of 3.4 Sv across that level, leaving a net upwelling of 2.8 Sv, small compared to the Ekman divergences noted in Section 5.4.2.

Overall the net upwelling in SODA for the northern hemisphere is 6.2 Sv, as prescribed by the cross-equatorial Ekman/Sverdrup transport following our discussion in Section 2.1 and in agreement with the cross-equatorial Somali Current transport. However, it is a difference of two large numbers, 21.0 Sv of total upwelling minus 14.8 Sv of downwelling. Only 0.9 Sv of the net Northern Hemisphere upwelling across the 75 m level occurs off Somalia, the major upwelling area of our study, while substantial net contributions originate in the interior, away from identified upwelling regions.

7. Observations of the equatorial roll in the Indian Ocean

As stated in the Introduction, the zonal-mean wind fields near the equator and model evidence (Miyama et al., 2002; Wacongne & Pacanowski, 1996) suggest that there should be a vertical-meridional overturning circulation within a narrow band around the equator, with northward (southward) surface currents on the equator during the summer (winter) monsoon and subsurface counterflow beneath. This counterflow should connect the southward (northward) Ekman transports (Fig. 5) from one side of the equator to the other during the summer (winter) monsoon. Here we present evidence from WOCE observations on the shallow cross-equatorial circulation with the focus on the situation under typical monsoonal windforcing conditions. As seen in Fig. 4c, the strongest cross-equatorial (northward) winds occur during the summer monsoon in the 45–60°E longitude band. At the same time, the meridional Ekman transport components on both sides

of the equator are southward in this longitudinal band which should, therefore, be a good testing area for the concept. In the winter monsoon season, climatological stress fields show regional cross-equatorial maxima south of Sri Lanka and over the western basin (Fig. 4a), but the meridional components on the equator are generally weak.

A number of interesting pieces of evidence on the shallow equatorial meridional circulation have been observed, by three different observational means: ADCP ship sections, a moored ADCP array and surface drifters. The data originate from the western basin, at 50–60°E, and there unfortunately only from the summer monsoon, from the eastern end during the winter monsoon, and from the central Indian Ocean south of Sri Lanka for both seasons.

Ship sections can only be used from the time period since the advent of ADCP technology, except for the now-classical *La Curieuse* outings, where currents were measured by a lowered rotor current-meter (Leetmaa & Stommel, 1980). Shipboard sections with conductivity–temperature–depth (CTD) and ADCP measurements were carried out at a number of longitudes during both monsoon seasons (Fig. 3). In the western basin, equatorial crossings were made by *Meteor* in June–July 1995 at 50°E and 56.5°E and again in August–September. There are other western summer monsoon sections from 1995 available in the ADCP Archive (http://ilikai.soest.hawaii.edu) but they were taken similar to ours in time and space and show the same result. One 1995 winter monsoon section from 95°E was found in the ADCP Archive and will be presented in the following (Fig. 3). At 80°E sections were carried out during the deployment and retrieval of a moored ADCP array (WOCE ICM-8; Reppin et al., 1999), by R/V *Sonne* in July 1993 and by R/V *Franklin* in August 1994.

In the following we first look at the western ship sections and then at the 95°E section, while the 80°E sections will be dealt with in conjunction with the moored ADCP array. From these sections, the best expectation for development of the equatorial roll is at 50°E during the summer monsoon, based on the climatological wind fields (Fig. 4) which show a focussed link of air flow between the SE Trades and the Findlater Jet (Fig. 4c). This core is concentrated near 48°E.

7.1. Western basin, 50–60°E

7.1.1. WOCE shipboard section measurements during the summer monsoon

In 1995 the monsoon was already well developed in June and lasted into September (Fig. 19). The zonal component was eastward north of the equator and westward south of it and the meridional component was northward throughout the equatorial belt and the entire monsoon season. In summary then, this is exactly the forcing situation that should be favourable for equatorial roll development.

The meridional currents along the four near-meridional *Meteor* sections in June–July and again in August/September are shown in Fig. 20. All four sections show there was a core of southward subsurface flow at 2°N–2°S and weak or northward surface flow above, all in agreement with the assumptions made. At the western sections, at 50°E, these cores are most pronounced. In early June, the near-surface flow on the equator was 40 cm s^{-1} northward, the subsurface core reached from 3°N to 2°S and decreased in velocity southward (Fig. 20a). During the period 31 August–2 September the subsurface core still existed with southward velocities exceeding 20 cm s^{-1}.

At the two eastern sections along 57.5°E, the cells were not as well organized as further west. In early July the cell was shallower, at a core depth of 40 m, and reached from 1.5°N to 0.5°S with velocities of only about 10–20 cm s^{-1}. In late August there was a much deeper core, at a depth of 150 m, which did not show a continuous pattern connecting it to the northern near-surface regions, as was the case further west at that time (Fig. 20b). It may had some origin other than Ekman driving. At the northern margins of the tropical zone there were indications of subsurface salinity maxima protruding into the equatorial zone in the individual sections.

An important question is whether the vertical overturing within the roll leads to diapycnal transfers.

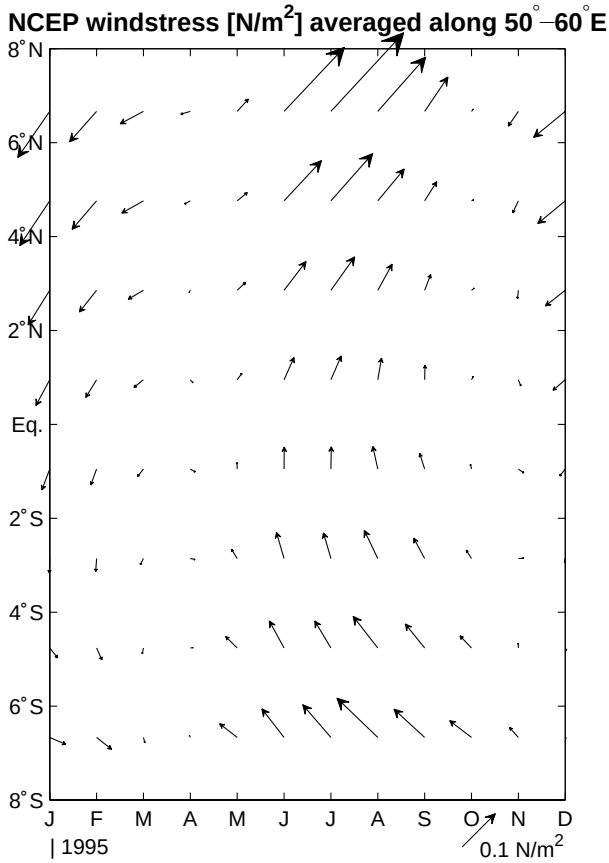

Fig. 19. Seasonal development of NCEP wind stresses during 1995 in 7°S–7°N latitude band, zonally averaged in 50°–60°E longitude range.

When plotting the temperature sections versus density, one can notice a slight cooling south of the equator but that may be caused by the pre-existing southward salinity decrease. Overall, the evidence resulting from the observations of Fig. 20 does not suggest that the equatorial roll causes noticeable diapycnal effects.

7.1.2. Earlier observations

Observational evidence on subsurface cross-equatorial flows was earlier presented from moored-station data by Knox (1976) and McPhaden (1982) and from shipboard measurements by Leetmaa and Stommel (1980). A section of repeat current profiling observations north of the Seychelles, along 55.5°E was carried out between February–May 1975 and again February–June 1976 by Leetmaa and Stommel (1980). The authors focussed primarily on the variability and meandering of the zonal currents but also addressed the meridional currents. They show one ‘conspicuous’ event during 15–26 May 1976 in conjunction with increasing northward winds during the month of May. The zonal equatorial winds during that time period were weak. In the two weeks a significant acceleration of southward flow was observed at depths of 70–100 m that reached through the entire latitude range covered, 3°S–2°N, while at the surface this flow was near-zero or northward. Interestingly, that acceleration approached the surface away from the equator in both Hemispheres, in agreement with the roll concept. During 1975 the authors reported an event of a strong northerly wind burst during which a strong northward flow was observed at the base of the mixed

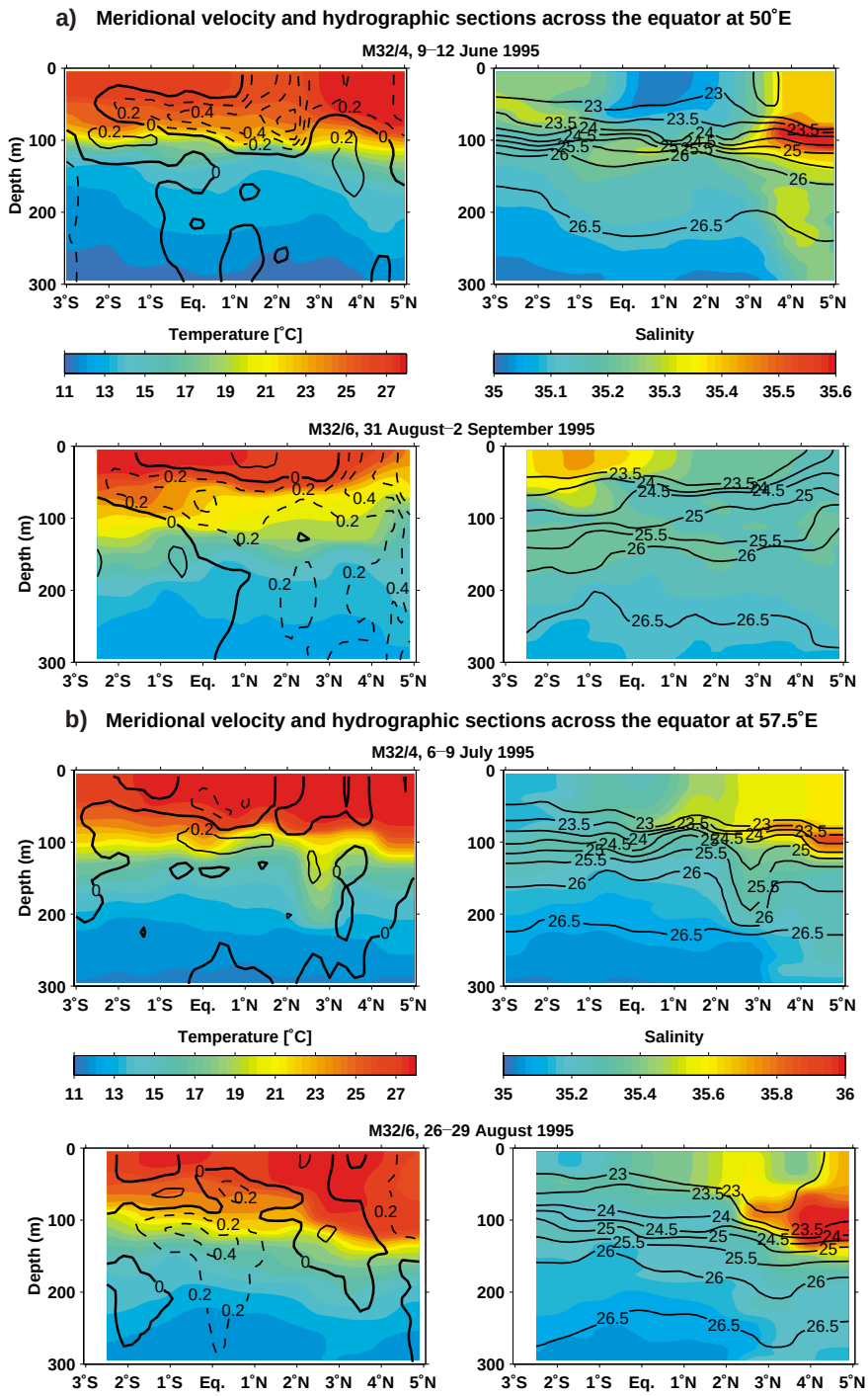

Fig. 20. Meridional currents and stratification in upper 300 m measured by shipboard ADCP and CTD along the four sections occupied by *Meteor* cruises M32/4 and M32/6 during the summer monsoon of 1995: (a) along 50°E during 9–12 June (top) and 31 August–2 September (bottom), (b) along 57.5°E during 6–9 July (top) and 26–29 August (bottom); shown on left hand side are meridional currents (contours) and salinity (colour) and on the right hand side potential density (contours) and temperature (colour).

layer. For both events, they commented on correlated changes further down, with a wavelength of about 170 m. They also noted that the EUC was almost completely eliminated during these meridional events.

The current meter time series near the island of Gan at 73°E, obtained by Knox (1976), were the first observations on the equator to cover an entire year, running from September 1973 to September 1974. Currents were measured by profiling current meter and were shown (in his Fig. 4) for the near-surface and about 70 m depth. There are a number of cases in the time series with significant meridional currents at thermocline level with at the same time small or near-zero meridional surface currents. In particular, during the entire winter monsoon of 1973–74, mid-November to mid-January, there was consistent southward flow of about 50 cm s^{-1} at 70 m and somewhat weaker (20 cm s^{-1}) southward surface flow, i.e. in agreement with the roll kinematics.

7.2. A winter monsoon section at 95°E

Inspection of the Joint Archive for Shipboard ADCP data (NOAA/NODC and University of Hawaii, http://ilikai.soest.hawaii.edu) yielded one winter monsoon section from the eastern Indian Ocean, the 95°E WOCE section (Hacker, Firing, Hummon, Gordon, & Kindl, 1998). The NCEP wind stresses for the time, 11–17 February 1995, were eastward north of the equator, westward south of it and were weak on the equator (Fig. 21a). The meridional currents now showed the reverse situation as for the western sections

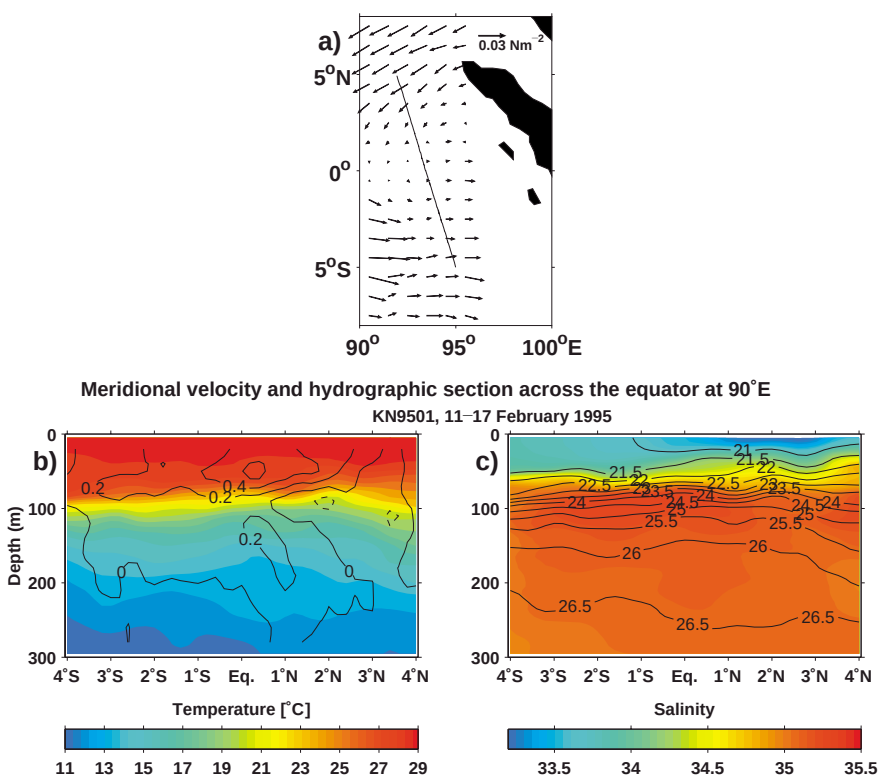

Fig. 21. Cross-equatorial ship section from R/V *Knorr* cruise KN 9501, taken during 11–17 February 1995 near 95°E (location see Fig. 3): (a) NCEP wind stress, (b) meridional current component (contours, northward is positive) and potential temperature (colours) showing northward subsurface flow across equator and (c) density (contours) and salinity (colours). (Courtesy of P. Hacker and P. Caldwell, http://ilikai.soest.hawaii.edu).

during the summer monsoon (Fig. 20), i.e. the presence of a northward subsurface core, with speeds exceeding 40 cm s^{-1} (Fig. 21b). A southward surface counterflow was not recognizable because of the absence of southward cross-equatorial winds. As in the previous observations, the bulk of the cross-equatorial flow was occurring above the pycnocline, although the flow encountered more stratified waters north of the equator (Fig. 21b,c).

7.3. WOCE moored current measurements at 80.5°E

WOCE moored array ICM8 was deployed from July 1993 to August 1994 with mooring positions on the equator and 45' to the south and north (Fig. 3). The moorings carried upward-looking ADCPs on top, covering the water column with velocity measurements between about 25 m and 300 m depth, in 8 m increments. The mooring motion, i.e. the blow-over of the ADCPs to larger depths in strong-current events, was compensated by reassembling depth bins for the further analysis. The array and the zonal currents and transports during the observational period have been discussed by Reppin et al. (1999). They reported a very strong eastward Wyrtki Jet in October–November 1993, a very weak spring jet in 1994 and the reappearance of the EUC in August–September 1994. The weak spring jet and anomalous EUC were, of course, the consequence of the anomalous easterlies of the 1994 'dipole' episode, discussed by Saji et al. (1999) and Vinayachandran et al. (1999), among others. Ship sections were taken at the beginning and at the end of the array observations. While in July 1993 the mixed layer between 3°S and 3°N was deep, at 90 m and the salinity maximum associated with the EUC was centred in the thermocline near 130 m (Fig. 22a–c). In September 1994 mixed-layer depths were shallow with a minimum of only 40 m on the equator (Fig. 22d–f).

Vector plots of zonally averaged NCEP wind stresses of 1993–94 for a 10° wide longitude range around 80°E show the situation we are looking for in both summer monsoons, with eastward winds to the north of the equator and westward winds to the south (Fig. 23). The northward stress component on the equator was positive during these two SW monsoon periods. However, due to the dipole anomaly the eastward winds during the 1994 summer monsoon north of the equator were weaker than in 1993.

During the 1993–94 winter monsoon, winds were anomalous due to the developing dipole episode, with strong eastward winds, lasting into January (Fig. 23). Under these circumstances the conditions for a reverse equatorial roll would not be met. From February to March 1994, zonal stresses on both sides of the equator resembled more what would be required for a winter monsoon equatorial roll (Fig. 23).

7.3.1. Currents during the summer monsoons of 1993 and 1994

Time series of the meridional current component for the upper 150 m show there were significant cross-equatorial currents throughout the year-long recording period (Fig. 24), many of them were obviously associated with shorter-period wave-type reversals. According to the wind situation of summer 1993, as discussed above, the current meter time series were averaged for the time period of 29 July (the beginning of the observations) to 29 September. Mean profiles from the three stations (K8—on the equator; K7—85 km to the north, and K9—85 km to the south) for that averaging period yielded northward flow on top and a southward core at 50–100 m depth at all three positions, with nearly equal maximum velocity of 20 cm s^{-1} at 70 m depth (Fig. 25a). This meridional profile is the anticipated situation from the earlier considerations. It was not just the result of a meandering of the westward undercurrent because it was a 45 day mean and it was consistent from 0°45'N to 0°45'S, i.e. over 170 km between the three ADCP moorings. The ship section of SO 88 (Fig. 22a–c) indicated that this meridional overturning motion was occurring within the mixed layer. A nearby mooring of PMEL/Seattle showed that this stratification with an about 90–100 m deep mixed layer continued throughout those 45 days of the initial averaging period (M. McPhaden, personal communication, 2000).

However, after the end of the summer monsoon wind stress situation characteristic for the roll develop-

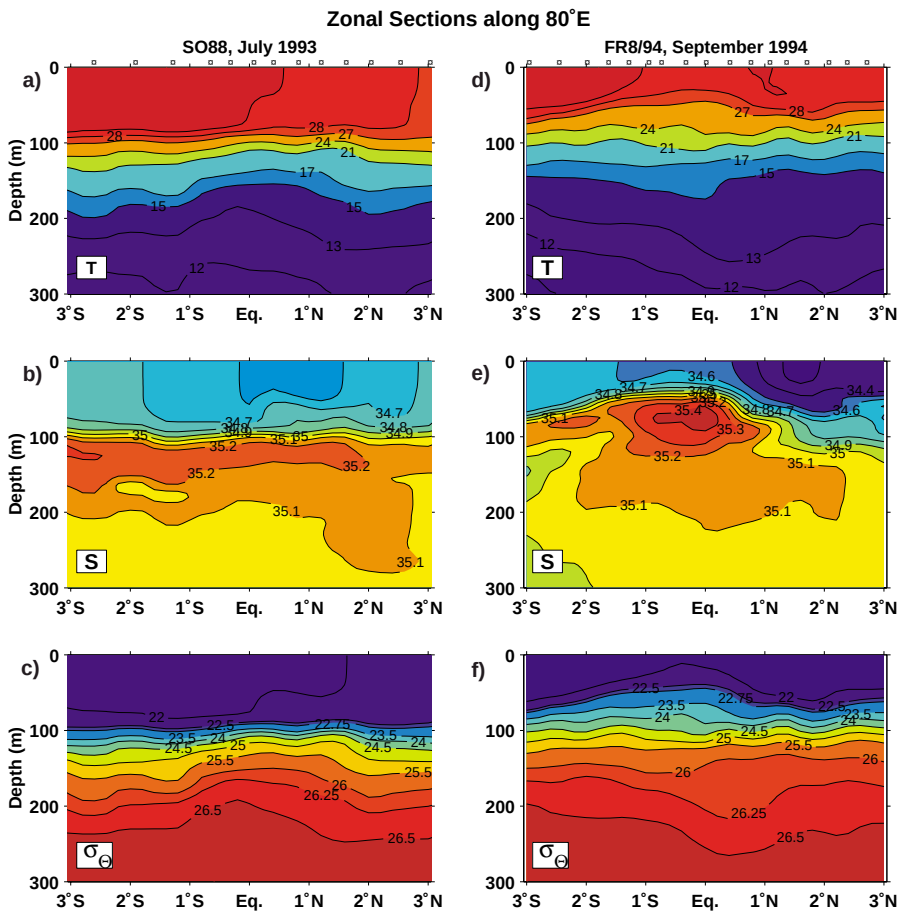

Fig. 22. Meridional sections of shipboard observations for upper 300 m along 80.5°E, 3°S–3°N, collected during deployment and retrieval of the moored ICM8 array, showing temperature (upper), salinity (middle) and potential density (bottom) from *Sonne* cruise SO 88 in July 1993 (left) and *Franklin* cruise FR 8/94 in September 1994 (right).

ment, the southward subsurface flow continued (Fig. 24) during November to December 1993, despite the wind now blowing parallel to the equator (Fig. 23), forcing the strong eastward Wyrtki Jet of late 1993 (Reppin et al., 1999; SM). A possible interpretation lies in the thermocline divergence associated with the Jet. During this time period southward subsurface flow was observed at station K9 located at 45' south of the equator, while northward currents were recorded at station K7, located at 45' north of the equator.

During the summer monsoon of 1994 the situation was anomalous due to the developing 'dipole' with westward equatorial wind anomalies and correspondingly the monsoon pattern was not as pronounced as in summer 1993. As already mentioned above, the mixed layer was much shallower, at only 40 m (Fig. 22d–f). The mean ADCP profiles for August–September (Fig. 25c) differ significantly from 1993. The first subsurface maximum shows southward flow with a maximum near 40 m, i.e. the bottom of the mixed layer measured when the ship passed at the end of that averaging period. Toward the surface, the shear was northward, in agreement with the summer monsoon roll situation. Below the mixed layer there was a second core of southward flow, centred at 130 m. Hence, the situation is unclear as to the roll physics, but if the top core is due to the fact that Ekman transport is passed from one side of the equator to the other; and it is again restricted to within the mixed layer.

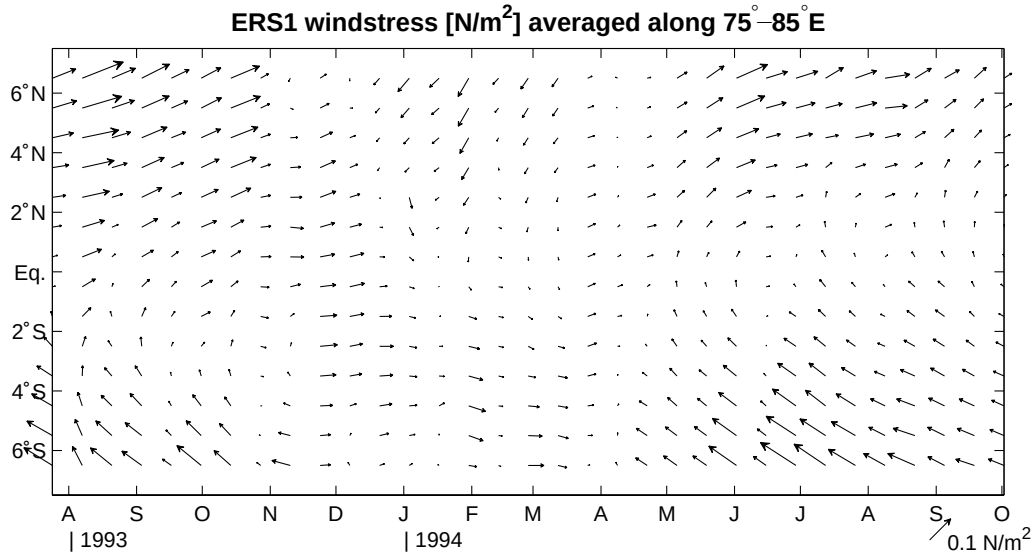

Fig. 23. NCEP wind stresses during 1993–94, zonally averaged in 75°–85°E longitude range.

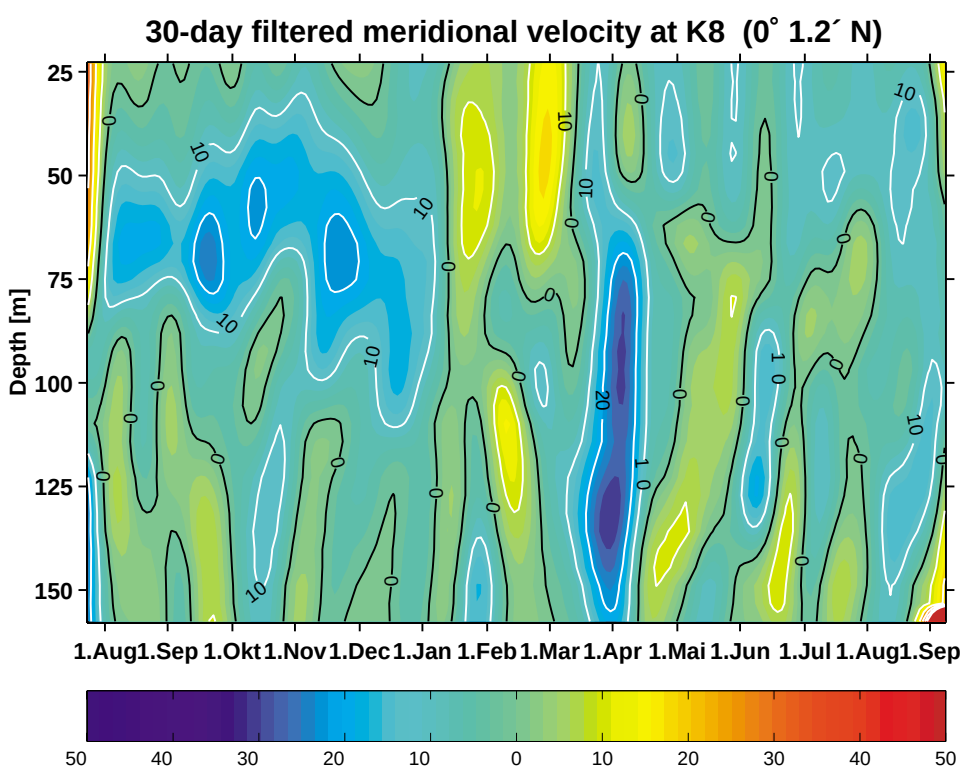

Fig. 24. Meridional currents in 25–150 m depth range from moored ADCP at Station K8, located at 80.5°E on the equator during August 1993–September 1994.

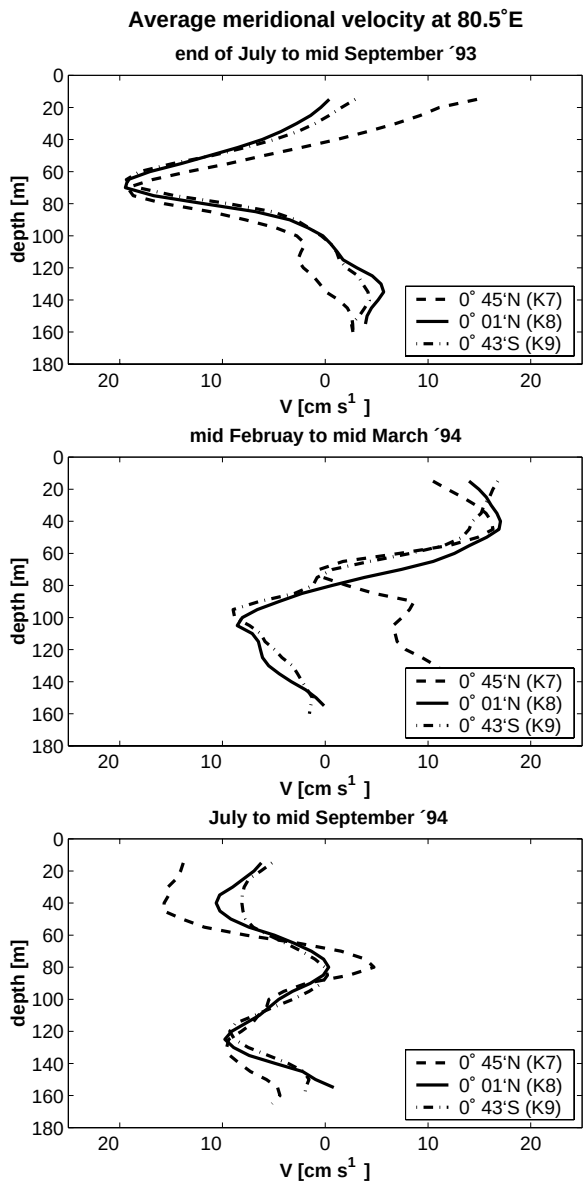

Fig. 25. ADCP current profiles of meridional velocity, averaged for (a) the summer monsoon of 1993 (29 July–29 September), showing equatorial roll with southward subsurface flow maximum at about 70 m depth, while near the surface currents are northward, (b) late winter monsoon of 1993/94 (20 February–15 March 1994), showing northward subsurface flow with maximum near 50 m depth with southward shear toward the surface, (c) the summer monsoon of 1994 (1 July–1 September) showing southward subsurface flow with maximum near 40 m and northward shear above.

7.3.2. Winter monsoon 1993/94

The beginning of the winter monsoon 1993/4 was marked by large eastward wind stress anomalies that reached far into both hemispheres (Fig. 23). A situation more typical for the winter monsoon was encountered in February–early March 1994 when there were northward Ekman transports on both sides of the equator and (weak) southward surface wind stress right on the equator. This was the only phase of persistent

northward cross-equatorial flow within the mixed layer (Fig. 24). Average meridional ADCP currents for 20 February–15 March showed a shallow northward subsurface current maximum at 40 m depth and southward shear above (Fig. 25b). However, this southward shear did not lead to actual southward surface flow, at least not in the depth range covered by the ADCPs, beginning at a depth of 25 m. The winds of that particular observational period were quite weak (Fig. 23), with maximum westward wind stress north of the equator only 0.04 N m^{-2} compared to 0.1 N m^{-2} during both summer monsoons covered in Fig. 23. Furthermore, the meridional component changed sign just south of the equator, rather than being negative throughout the equatorial zone as was the case for the reverse summer situation. As mentioned, this period was one of a developing strong equatorial anomaly.

In summary, although the observation period 1993/94 of the moored array fell into an anomaly episode with untypical monsoon winds, the ADCP profiles for the two summer and one winter monsoon season were in overall agreement with the equatorial roll concept, with the summer 1993 the strongest and the winter of 1994 the weakest case. The combined stratification and ADCP evidence suggests that the equatorial roll is dominantly confined to the mixed layer, i.e. that it is of no or little relevance for diapycnal fluxes and the heat budget.

7.4. Drifter trajectories at the equator

Drifter tracks from the equatorial Indian Ocean were evaluated regarding cross-equatorial surface flows during both monsoon seasons. The distribution was quite uneven and sparse, with no coverage of the western equatorial zone during the winter monsoon and very sparse coverage of the western half during the summer monsoon. The drifter velocities have been averaged in 0.5° latitude bins over the width of the interior ocean, longitude range 38°–110°E and for the months of July–September (summer monsoon) and December to February (winter monsoon).

The resulting zonal current components for both monsoon seasons (Fig. 26a) show the expected zonal currents in comparison with the schematic climatological presentations of Figs. 1 and 2. The eastward SECC in the 3–6°S band is the most conspicuous feature during the winter monsoon. North of the equator the SW Monsoon Current flowed eastward in summer and the NE Monsoon Current flowed westward in winter.

In the meridional profiles we see the predicted latitudinal profiles for the winter monsoon Ekman transport and surface expression of the equatorial roll (Fig. 26b): the meridional component is northward on both sides of the equator and southward on the equator. This does not systematically change, if only drifters out of the western (50°–75°E) or eastern (75°–100°E) part of the basin are used. For the summer monsoon, the surface currents were southward on either side of the equator (Fig. 26b), as expected; directly on the equator the meridional currents were zero, i.e. the relative profile is in agreement with the assumption but the absolute current was not directed against the Ekman flow.

In summary it can be stated that despite the fairly sparse data base the drifter analysis supports the existence of the equatorial roll.

7.5. The equatorial roll in SODA

The SODA model, with its 15 m vertical resolution of the upper ocean, reproduces the equatorial roll and its seasonal reversal. For the summer monsoon (Fig. 27a) the most strongly developed overturning cell in the model circulation occurs between 50° and 60°E, due to the strong cross-equatorial windstress of the Findlater Jet. The intensity of the subsurface southward core in that zone is -40 cm s^{-1}, which is in agreement with the observations of our western-basin ship sections (Fig. 20). In the interior and eastern domain, the subsurface southward flow is 10 cm^{-1} or less, and the northward surface flow is weak. The cross-equatorial transports during the summer monsoon are large, with a net of -37.3 Sv for the top 100 m, in agreement with the magnitude of the near-equatorial Ekman and Sverdrup transports (see Section

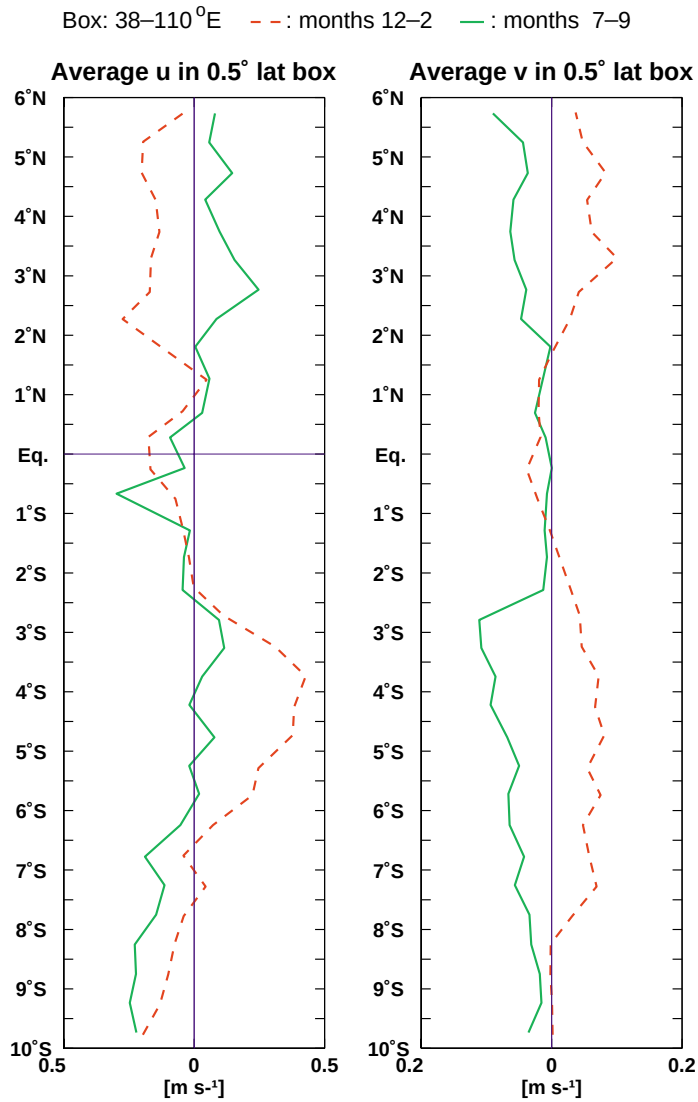

Fig. 26. Zonal-mean meridional profiles of surface velocities from drifter trajectories (courtesy C. Sena-Martins) for the equatorial Indian Ocean, between 10°S and 6°N for (a) zonal and (b) meridional current components; solid curves are for summer monsoon (July–September), dashed for winter monsoon (December–February).

2.1 and SM). The summer monsoon overturning transport by the roll amounts to 10 Sv, where it has to be noted that this amount excludes most of the Somali Current, because the integration was only carried out for the section east of 44.5°E.

The somewhat weaker reverse situation occurs in January, at the height of the winter monsoon (Fig. 27b), again in correspondence with the weaker equatorial Sverdrup and Ekman transports of the winter monsoon (SM). The net northward transport in the upper 100 m is now 18.5 Sv and the roll overturning transport is −12.1 Sv. For the annual mean (Fig. 27c), the shallow overturning is dominated by the summer monsoon roll, with weak northward surface currents and weak southward subsurface currents that have their maximum at about 55°E. The net cross-equatorial transport of the upper 100 m is −9.4 Sv.

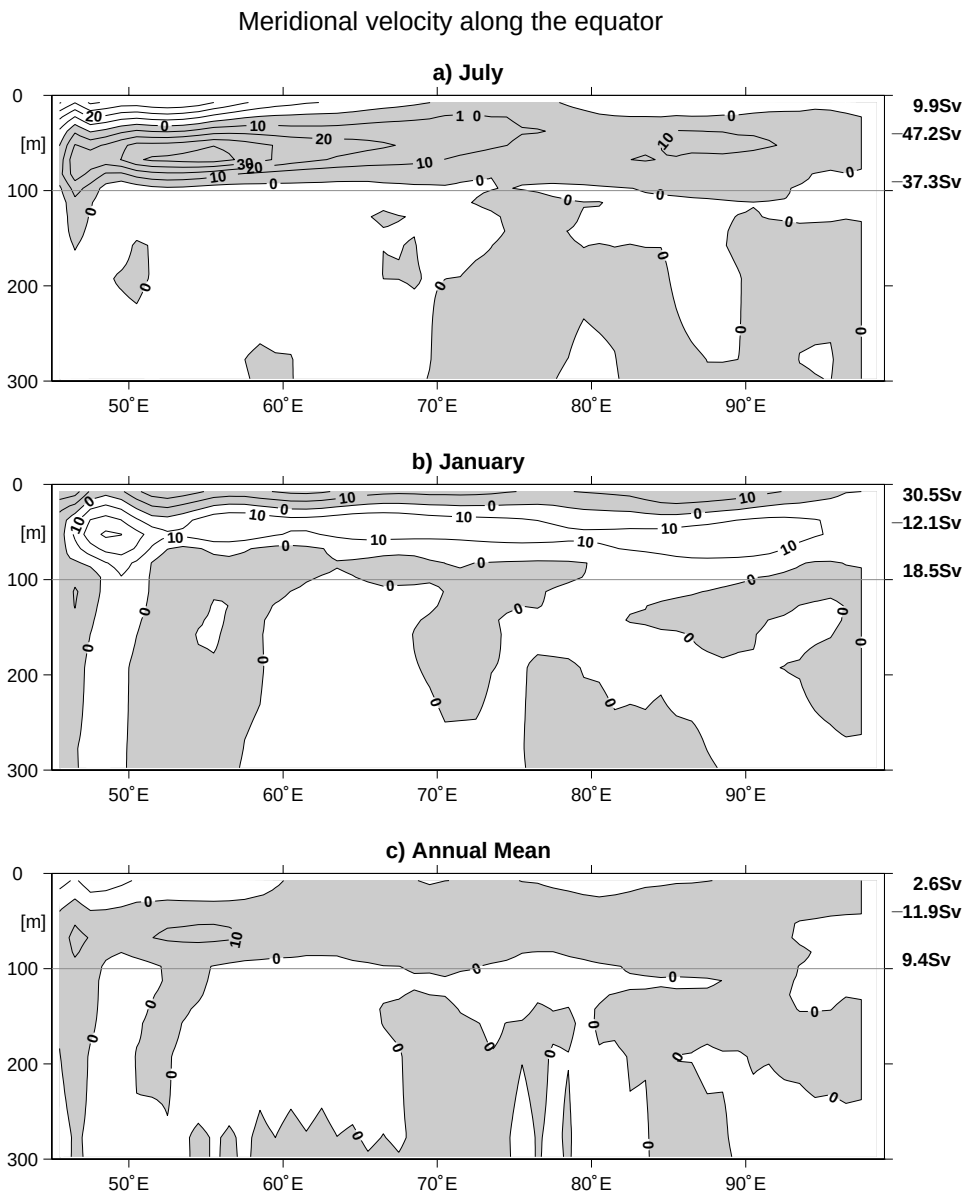

Fig. 27. The equatorial roll in the SODA model, shown by the meridional velocities (cm s^{-1}; positive is northward) along the equator for (a) July, (b) January and (c) annual mean. Also shown (right margin) are northward, southward and net transports in 0–100 m layer.

8. Summary and conclusions

The shallow overturning circulation of the Indian Ocean differs drastically from the subtropical cells (STCs) of the other two major oceans, because the Indian Ocean does not possess an equatorial upwelling regime. In the Indian Ocean, subduction occurs dominantly in the Southern Hemisphere and upwelling in the Northern Hemisphere, in the Somali and Arabian coastal upwelling areas, leading to a cross-equatorial

shallow cell. The return flow from northern upwelling to southern subduction occurs by southward cross-equatorial Ekman transport, involving a near-surface meridional overturning roll on the equator. This circulation pattern is confined to the summer monsoon season but determines the annual-mean circulation. In the preceding sections we discussed the observational evidence for the sources, pathways and sinks of the Indian Ocean STC, as summarized schematically in Fig. 28, and compared it to Ekman and Sverdrup transports derived from the windstress fields as well as results from the Simple Ocean Data Assimilation (SODA; Carton et al., 2000).

The subsurface STC pathways are identified by the distributions of salinity and nutrients on shallow isopycnals that surface in the main upwelling areas of the northern Arabian Sea, showing a connection from the Indonesian Throughflow regime and subtropical Indian Ocean into the western boundary and onward across the equator with the Somali Current. The role of the Mozambique Current as a water mass route connecting the Throughflow with the southern Indian Ocean has been emphasized in recent inverse model studies (e.g. Ganachaud et al., 2000). Evidence from drifter and mid-level float trajectories as well as earlier regional budget studies (Swallow et al., 1991) suggest that the near-surface SEC flow arriving north of Madagascar mostly continues northwestward toward the East African Coast Current and Somali Current (Fig. 28) while the thermocline flow supplies the Mozambique Channel throughflow. This throughflow is to some extent carried by southward propagating eddies (de Ruijter et al., 2002). In the density

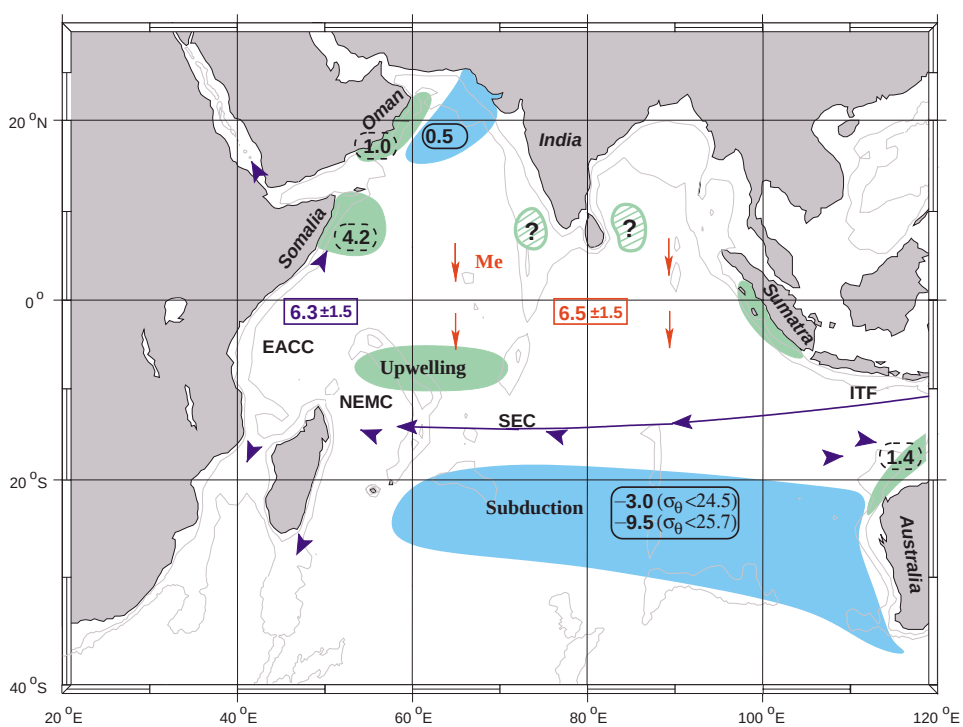

Fig. 28. Schematic presentation of circulation involved in connecting subduction regions of the southern hemisphere with Indian Ocean upwelling regions. Subduction amount in Southern Hemisphere is for densities (Karstensen & Quadfasel, 2002) that can upwell off Somalia during weaker and stronger upwelling cases. Cross-equatorial Somali Current transport for upwelling density range is based on earlier array measurements of Schott et al. (1990). Upwelling off Somalia is estimated from WOCE ship sections 1993 and 1995. NW Australian upwelling is after Godfrey and Mansbridge (2000). See text for details. There is an approximate balance for the main STC between the independent estimates of cross-equatorial subsurface northward Somali Current transport, of Somali upwelling and of southward Ekman/Sverdrup return flow across the equator.

range relevant for upwelling, about 6 Sv are estimated to flow northward across the equator based on moored current meter observations in the Somali Current (Schott et al., 1990).

Regarding subduction in the southern hemisphere, Karstensen and Quadfasel (2002) recently estimated from an analysis of climatological data that a total of 34 Sv is subducted into density classes 23–27 kg m^{-3} . Out of these, 9.5 Sv enter into densities <25.7 kg m^{-3} , corresponding to about 150 m upwelling depth off Somalia. The upwelling, as observed during the coast-parallel WOCE cruises of 1995, came from lower densities, <24.5 kg m^{-3} for which the subduction result of Karstensen and Quadfasel (2002) was 3.0 Sv (Fig. 28). The denser water masses subducted further south are carried westward with the South Equatorial Current and then flow southward, partially retroflecting southeast of Madagascar, partially continuing toward the Agulhas and supplying Agulhas eddies that propagate across the South Atlantic. The Indian Ocean shallow cell thus is in its majority intertwined with the STCs of the other two oceans.

Some subduction, estimated at about 0.5 Sv in the annual mean by Karstensen (personal communication, 2001), also happens in the northern Arabian Sea during the winter monsoon in density classes that can upwell in the region (Fig. 28). A similar amount of surface water is transformed into thermocline waters in the Red Sea and Arabian Gulf, but into density classes of 27.2 and 26.6 kg m^{-3}, respectively, i.e. water that is too dense for upwelling.

Somali upwelling occurs at the offshore-flowing flanks of the Southern Gyre at 3–5°N and of the Great Whirl (Figs. 14 and 15), with the GW outflow partially leaving northward through the passage between Socotra and the African continent and partly recirculating southeastward, while taking up heat and losing density. From WOCE sections off Somalia in 1993 and 1995 we determine the SG outflow of upwelled water during the summer monsoon at 8.7 Sv. For the GW outflow we obtain 2.1 Sv through the Socotra Passage into the Gulf of Aden and 10.3 Sv eastward into the 7–10°N range where the upwelled waters warm and recirculate back into the boundary regime at shallower densities. Taking these values as typical for the 4 months long summer monsoon season yields an annual mean upwelling of 7 Sv from the combined SG and GW upwelling. However, we consider this a high estimate, since some of this offshore flow will slump back into the thermocline and does not become transformed into surface water. From heat flux considerations we estimate that only the lighter fractions of the offshore flow can be warmed enough during the course of the monsoon to become surface waters. This yields a total upwelling rate of 12.5 Sv for the summer monsoon or 4.2 Sv as an annual mean. The offshore Ekman transport from the NCEP and ERS-1/2 climatologies was determined at 19.5 ± 5.1 Sv, and 16.2 ± 4.0 Sv, respectively, for the summer monsoon, supporting the high estimate more than the conservative one.

For the Arabian coast it was found that upwelling occurs by filaments connected to topographic features that carry the upwelled waters far out into the interior of the Arabian Sea (Fischer et al., 2002). From different pieces of evidence this upwelling is estimated at about 3 Sv for the monsoon season or 1 Sv annually.

There is also open ocean upwelling in the Indian Ocean. Upwelling in the open Arabian Sea has meanwhile been discounted as a source since it is by far dominated by local mixed-layer deepening during the summer monsoon (Lee et al., 2000). However, northern-hemispheric open-ocean upwelling is emphasized in the model study of Miyama et al. (2002), related to the cyclonic domes east and west of southern India and Sri Lanka. This upwelling is also supported by Ekman divergences.

There are also indications for open-ocean upwelling in the 5–10°S latitude range, which is marked by doming of the thermocline (Fig. 11) at the northern edge of the Trade wind regime. This upwelling, while not recognisable in SST maps because it is masked by the general meridional temperature increase in that region, is suggested by satellite colour images that show a chlorophyll maximum in that region. Furthermore, the Ekman divergence estimates are almost 10 Sv for the zone 2–12°S, 50–90°E. This upwelling will not involve the cross-equatorial cell; it will close a southern overturning cell, supplied by southern subduction and Indonesian Throughflow (Fig. 28).

There are two other upwelling regimes at the eastern Indian Ocean margin that can, at least at times,

contribute considerably to the shallow overturning circulation. One aspect is the role of eastern tropical upwelling during 'dipole' episodes, which are marked by westward wind anomalies along the equator and significant uplifting of the thermocline and SST reduction along the eastern equatorial band and off Sumatra. Two such episodes occurred during the WOCE period, in 1994 and 1997. The Ekman divergence in the eastern equatorial band within 3°N and 3°S during both these episodes exceeded 20 Sv, the 20 °C isotherm rose by 60 m in the east (Fig. 7), leading to thermocline waters being exposed to air–sea exchanges. A similar amount was derived from SODA for the 1997 episode. On the other hand, NCEP fluxes do not reveal significant heat fluxes during a dipole episode, meaning that much of the thermocline water does not become transformed into lighter surface waters, but returns into the stratification when the thermocline relaxes at the end of the 'dipole' episode. Assuming for an upper limit that the entire 20 Sv that upwell over a two months period of the thermocline shallowing (Fig. 7) of such an anomaly become transformed into surface waters, and taking the repetition time of such events at 5 years, yields a mean annual upwelling rate of 0.7 Sv, but the real number would be less.

The second regime is the northwest Australian shelf and Arafura Sea, for which Godfrey and Mansbridge (2000) established Ekman and geostrophic budgets. On their basis, an annual-mean estimate of 1.4 Sv for the combined region followed (Fig. 28).

The constraints for the cross-equatorial cell are fairly well defined (Fig. 28): we obtain 6.3 Sv of northward Somali Current flow across the equator in the depth range that can supply upwelling and we estimate the error on this number at ±1.5 Sv (Fig. 28); and for the shallow wind-driven southward cross-equatorial return flow the Sverdrup transport from both climatologies yields 6.5 Sv (Fig. 28), also with an error estimate of ±1.5 Sv as an average for both climatologies (as discussed by Miyama et al., 2002 and Godfrey et al. (2001), the cross-equatorial Sverdrup transports are similar to the near-equatorial Ekman transports due to the peculiarities of the Indian Ocean wind fields).

Overall, we estimate a total of about 5 Sv for the Somali and Arabian upwelling regimes combined. In contrast to our estimates and the large offshore Ekman transport off Somalia, the model study of Miyama et al. (2002) and our analysis of the SODA model (Fig. 17) finds a relatively small role of net Somali upwelling in the cross-equatorial cell. Instead, significant contributions are by open-ocean upwelling in the cyclonic domes on both sides of India and Sri Lanka. Models also show large upwelling/downwelling transports in other identified northern upwelling areas that need to be explained. For example, in SODA these transports across the 75 m level are 21.0 Sv/−14.6 Sv for the entire Northern Hemisphere (Fig. 18), which are more than double the net upwelling rate. These exchanges are somewhat smaller for layer models like that of McCreary et al. (1993) but still much larger than the net upwelling rate (Miyama et al., 2002).

A challenging result of the Miyama et al. (2002) trajectory analysis from a high-resolution numerical model is that upwelling particles crossed the equator with the Somali Current at quite deep levels, 300 m and more, corresponding to temperatures of some 12 °C. What are the physical mechanisms in such models that make these deep waters rise to the surface?

We have studied in some detail equatorial roll as part of the shallow overturning circulation that forms the link between the southern supply and the northern upwelling regimes, based on own and earlier equatorial measurements. We could clearly establish the existence of the subsurface flow of the roll, exceeding 20 cm s^{-1} from shipboard ADCP sections taken during the summer monsoon in the western basin where strong northward winds on the equator as well as southward Ekman transports in both hemispheres generate ideal conditions for its existence. The SODA output supports the existence of the equatorial roll is best developed at 50–60°E during the summer monsoon (Fig. 27). Evidence for the reverse situation for the winter monsoon is also presented but the roll was not as well developed, probably because the lack of southward winds on the equator during our available observations.

Whether the rolls cause diapycnal fluxes depends on whether they penetrate through the bottom of the mixed layer. It does not occur in models of low vertical resolution because their rolls are contained in the mixed layer and so have no effect on the heat budget (e.g. McCreary et al., 1993; Miyama et al., 2002).

Schiller, Godfrey, McIntosh, Meyers, and Wijffels (1998) commented on the diapycnal fluxes of the cells in their GCM with high vertical resolution. They found that when the mixed-layer depth was less than the vertical scale of the equatorial roll, which was the case in May in their simulation, there was a band of heat uptake by the upwelled water south of the equator. In our observations however, the evidence points to the roll being predominantly restricted to the surface-mixed layer or at least uppermost part of the thermocline, leading to the conclusion that the equatorial roll has small diapycnal effects is therefore of little consequence for the meridional heat transport. Additional work has now to determine what the relation between the net southward Ekman/Sverdrup transport on the equator versus the northward surface return flow is within the roll and whether a simple parameterisation can be derived.

Acknowledgements

This paper is based on a presentation prepared for the CLIVAR STC Workshop in Venice, October 2000, and the incentive of Paola Malanotte-Rizzoli in getting us all working on digesting observations and models for the global STCs is much appreciated. We thank H. Bezdec of NOAA/AOML and C. Sena-Martins of IfM Kiel for help in the drifter track analysis, and A. Fischer, (LODYC, Paris) for information on recent observations of the Oman filament observations. The ADCP section of *Knorr* cruise KN 9501 (Fig. 21) was obtained from the Joint Archive for Shipboard ADCP-NOAA/NODC and University of Hawaii, courtesy Peter Hacker and Pat Caldwell (http://ilikai.soest.hawaii.edu), for the corresponding CTD data we acknowledge Arnold Gordon. We thank Jim Carton (U. Maryland) for making available the output fields of his SODA model. Helpful discussions with Julian McCreary and his cooperators during a visit at IPRC (U. Hawaii) on model STCs and constructive comments by two anonymous reviewers are also acknowledged. This study was supported by the German Bundesministerium für Bildung Wissenschaft und Forschung (BMBF) as part of the German CLIVAR/marin program, contract 03F0246A.

References

Behera, S. K., & Yamagata, T. (2001). Subtropical SST dipole events in the southern Indian Ocean. *Geophysical Research Letters*, *28*, 327–330.

Böhm, E., Morrison, J. M., Manghnani, V., Kim, H. -S., & Flagg, C. N. (1999). The Ras al Hadd Jet: remotely sensed and acoustic Doppler current profiler observations in 1994–1995. *Deep-Sea Research II*, *46*, 1531–1549.

Carton, J. A., Chepurin, G., Cao, X., & Giese, B. (2000). A simple ocean data assimilation analysis of the global upper ocean 1950–95. Part I: Methodology. *Journal of Physical Oceanography*, *30*, 294–309.

Chereskin, T. K., Wilson, W. D., Bryden, H. L., Field, A., & Morrison, J. (1997). Observations of the Ekman balance at 8°30′N in the Arabian Sea during the 1995 southwest monsoon. *Geophysical Research Letters*, *24*, 2541–2544.

da Silva, A. M., Young, C. C., & Levitus, S. (1994). *Atlas of surface marine data 1994: Vol. 3. Anomalies of heat and momentum fluxes. Vol. 4. Anomalies of fresh water fluxes.* NOAA Atlas NESDIS 8 (413 pp.). US Department of Commerce, NOAA, NESDIS.

de Ruijter, W. P. M., Ridderinkhof, H., Lutjeharms, J. R. E., & Schouten, M. W. (2002). Direct observations of the flow in the Mozambique Channel. *Geophysical Research Letters*, in press.

Di Marco, S. F., Chapman, P., Nowlin, W. D. Jr., Hacker, P., Donahue, K., Luther, M., Johnson, G. C., & Toole, J. (2001). Volume transport and property distribution in the Mozambique Channel. *Deep-Sea Research II*, *49*, 1481–1521.

Düing, W., & Schott, F. (1978). Measurements in the source region of the Somali Current during the monsoon reversal. *Journal of Physical Oceanography*, *8*, 278–289.

Fischer, A. S., Weller, R. A., Rudnick, D. L., Eriksen, C. C., Lee, C. M., Brink, K. H., Fox, C. A., & Leben, R. R. (2002). Mesocale eddies, costal upwelling, and the upper ocean heat budget in the Arabian Sea. *Deep-Sea Research II*, *49*(12), 2231–2264.

Fischer, J., Schott, F., & Stramma, L. (1996). Currents and transports of the Great Whirl–Socotra Gyre System during the Summer Monsoon August, 1993. *Journal of Geophysical Research*, *101*, 3573–3587.

Ganachaud, A., Wunsch, C., & Marotzke, J. (2000). The meridional overturning and large-scale circulation of the Indian Ocean. *Journal of Geophysical Research*, *105*, 26117–26134.

Garternicht, U., & Schott, F. (1997). Heat fluxes of the Indian Ocean from a global eddy-resolving model. *Journal of Geophysical Research, 102*, 21147–21159.

Godfrey, J. S., Johnson, G. C., McPhaden, M. J., Reverdin, G., & Wijffels, S. (2001). The tropical ocean circulation. In J. Church, J. Gould, & G. Siedler (Eds.), *Ocean circulation and climate* (pp. 215–245). London: Academic Press.

Godfrey, J. S., & Mansbridge, J. V. (2000). Ekman transports, tidal mixing and the control of temperature structure in Australia's northwest waters. *Journal of Geophysical Research, 105*, 24021–24044.

Hacker, P., Firing, E., Hummon, J., Gordon, A., & Kindl, J. C. (1998). Bay of Bengal currents along the northeast monsoon. *Geophysical Research Letters, 25*, 2769–2772.

Hellerman, S., & Resenstein, M. (1983). Normal monthly wind stress over the world ocean with error estimates. *J. Phys. Oceanogr., 13*, 1093–1105.

Josey, S. A., Kent, E. C., & Taylor, P. K. (1999). New insights into the ocean heat budget closure problem from analysis of the SOC air–sea flux climatology. *Journal of Climate, 12*, 2856–2880.

Karstensen, J., & Quadfasel, D. (2002). Water subducted into the Indian Ocean. *Deep-Sea Research II, 49*, 1441–1458.

Knox, R. (1976). On a long series of measurements of Indian Ocean equatorial currents near Addu Atoll. *Deep-Sea Research, 23*, 211–221.

Koske, P. (1972). Hydrographische Verhältnisse im Persischen Golf aufgrund von Beobachtungen von FS Meteor im Frühjahr 1965. *Meteor Forschungsergebnisse, A11*, 58–73.

Lee, C. M., Jones, B. H., Brink, K. H., & Fischer, A. S. (2000). The upper ocean response to monsoonal forcing in the Arabian Sea: seasonal and spatial variability. *Deep-Sea Research II, 47*, 1177–1226.

Lee, T., & Marotzke, J. (1998). Seasonal cycles of meridional overturning and heat transport of the Indian Ocean. *Journal of Physical Oceanography, 28*, 923–943.

Leetmaa, A., & Stommel, H. (1980). Equatorial current observations in the western Indian Ocean during 1975 and 1976. *Journal of Physical Oceanography, 10*, 258–269.

Levitus, S., & Boyer, T. (1994a). *World ocean atlas 1994. Vol. 3. Salinity*. NOAA Atlas NESDIS 3 (93 pp.). Washington, DC: US Government Printing Office.

Levitus, S., & Boyer, T. (1994b). *World ocean atlas 1994. Vol. 4. Temperature*. NOAA Atlas NESDIS 4 (117 pp.). Washington, DC: US Government Printing Office.

Marshall, J. C., Nurser, A. J. G., & Williams, R. G. (1993). Inferring the subduction rate and period over the North Atlantic. *Journal of Physical Oceanography, 23*, 1315–1329.

McCarthy, M. C., & Talley, L. D. (1999). Three-dimensional isoneutral potential vorticity structure in the Indian Ocean. *Journal of Geophysical Research, 104*, 13251–13268.

McCartney, M. S. (1982). The subtropical recirculation of Mode Waters. *Journal of Marine Research, 40*(Suppl.), 427–464.

McCreary, J. P., Jr., Kundu, P. K., & Molinari, R. L. (1993). A numerical investigation of dynamics, thermodynamics and mixed layer processes in the Indian Ocean. *Progress in Oceanography, 31*, 181–244.

McPhaden, M. (1982). Variability in the central Indian Ocean. Part I: Ocean dynamics. *Journal of Marine Research, 40*, 157–176.

Miyama, T., McCreary, J. P., Jensen, T. G., Loschnigg, J., Godfrey, S., & Ishida, A. (2002). Structure and dynamics of the Indian Ocean cross-equatorial cell. *Deep-Sea Research II*, accepted.

Morrison, J. M. (1997). Intermonsoonal changes in the T–S properties of the near-surface waters of the northern Arabian Sea. *Geophysical Research Letters, 24*, 2553–2556.

Murray, S. P., & Johns, W. (1997). Direct observations of seasonal exchange through the Bab el Mandab Strait. *Geophysical Research Letters, 24*, 2557–2560.

Murtugudde, R., McCreary, J. P., & Bugalacchi, A. J. (2000). Oceanic processes associated with anomalous events in the Indian Ocean with relevance to 1997–1998. *J. Geophys. Res., 105*, 3295–3306.

Murtugudde, R., Signorini, S., Christian, J., Busalacchi, A., McClain, C., & Picaut, J. (1999). Ocean color variability of the tropical Indo-Pacific basin observed by SeaWiFS during 1997–98. *Journal of Geophysical Research, 104*, 18351–18366.

Philander, G., & Pacanowski, R. C. (1981). Response of equatorial oceans to periodic forcing. *Journal of Geophysical Research, 86*, 1903–1916.

Reason, C. J. C., & Mulenga, H. M. (1999). Relationships between South African rainfall and SST anomalies in the SW Indian Ocean. *International Journal of Climatology, 19*, 1651–1673.

Reppin, J., Schott, F. A., Fischer, J., & Quadfasel, D. (1999). Equatorial currents and transports in the upper central Indian Ocean: annual cycle and interannual variability. *Journal of Geophysical Research, 104*, 15495–15514.

Saji, N. H., Goswami, B. N., Vinayachandran, P. N., & Yamagata, T. (1999). A dipole in the tropical Indian Ocean. *Nature, London, 401*, 360–363.

Schiller, A., Godfrey, J. S., McIntosh, P. C., Meyers, G., & Wijffels, S. E. (1998). Seasonal near-surface dynamics and thermodynamics of the Indian Ocean and Indonesian Throughflow in a global ocean general circulation model. *Journal of Physical Oceanography, 28*, 2288–2312.

Schott, F. (1983). Monsoon response of the Somali Current and associated upwelling. *Progress in Oceanography, 12*, 357–381.

Schott, F., & Fischer, J. (2000). Winter monsoon circulation of the northern Arabian Sea and Somali Current. *Journal of Geophysical Research, 105*, 6359–6376.

Schott, F., Fischer, J., Garternicht, U., & Quadfasel, D. (1997). Summer monsoon response of the Northern Somali Current, 1995. *Geophysical Research Letters, 24*, 2565–2568.

Schott, F., & McCreary, J. Jr. (2001). The monsoon circulation of the Indian Ocean. *Progress in Oceanography, 51*, 1–123.

Schott, F., Swallow, J. C., & Fieux, M. (1990). The Somali Current at the equator: annual cycle of currents and transports in the upper 1000 m and connection to neighbouring latitudes. *Deep-Sea Research, 37*, 1825–1848.

Shankar, D., & Shetye, S. R. (1997). On the dynamics of the Lakshadweep high and low in the southeastern Arabian Sea. *Journal of Geophysical Research, 102*, 12551–12562.

Shankar, D., Vinayachandran, P. N., Unnikrishnan, A. S., & Shetye, S. R. (2002). The monsoon currents in the north Indian Ocean. *Progress in Oceanography, 52*(1), 63–119.

Shetye, S. R., Gouveia, A. D., Shenoi, S. S. C., Sundar, D., Michael, G. S., Almeida, A. M., & Santanam, K. (1990). Hydrography and circulation off the west coast of India during the Southwest Monsoon, 1987. *Journal of Marine Research, 48*, 359–378.

Shetye, S. R., Shenoi, S. S. C., Gouveia, A. D., Michael, G. S., Sundar, D., & Nampoothiri, G. (1991). Wind-driven coastal upwelling along the western boundary of the Bay of Bengal during the southwest monsoon. *Continental Shelf Research, 11*, 1397–1408.

Shi, W., Morrison, J. M., Böhm, E., & Manghnani, V. (2000). The Oman upwelling zone during 1993, 1994 and 1995. *Deep-Sea Research II, 47*, 1227–1247.

Smith, R. L., & Bottero, J. S. (1977). On upwelling in the Arabian Sea. In M. V. Angel (Ed.), *A voyage of discovery* (pp. 291–304). New York: Pergamon Press.

Song, Q., & Gordon, A. (2002). Indonesian Throughflow water pathways in the Western Indian Ocean. *Deep-Sea Research II*, submitted.

Stramma, L., & Lutjeharms, J. R. E. (1997). The flow field of the subtropical gyre of the South Indian Ocean. *Journal of Geophysical Research, 102*, 5513–5530.

Susanto, D. R., & Gordon, A. L. (2001). Upwelling along the coasts of Java and Sumatra and its relation to ENSO. *Geophysical Research Letters, 28*, 1599–1602.

Swallow, J. C., & Bruce, J. C. (1966). Current measurements off the Somali coast during the southwest monsoon of 1964. *Deep-Sea Research, 13*, 861–888.

Swallow, J. C., Fieux, M., & Schott, F. (1988). The boundary currents east and north of Madagascar, Part I: Geostrophic currents and transports. *Journal of Geophysical Reserch, 93*, 4951–4962.

Swallow, J. C., Schott, F., & Fieux, M. (1991). Structure and transport of the East African Coastal Current. *Journal of Geophysical Research, 96*, 22254–22267.

Vinayachandran, P. N., Saji, N. H., & Yamagata, T. (1999). Response of the Equatorial Indian Ocean to an unusual wind event during 1994. *Geophysical Research Letters, 26*, 1613–1616.

Vinayachandran, P. N., & Yamagata, T. (1998). Monsoon response of the sea around Sri Lanka: generation of thermal domes and anticyclonic vortices. *Journal of Physical Oceanography, 28*, 1946–1960.

Wacongne, S., & Pacanowski, R. (1996). Seasonal heat transport in a primitive equations model of the tropical Indian Ocean. *Journal of Physical Oceanography, 26*, 2666–2699.

Webster, P. J., Moore, A. M., Loschnigg, J. P., & Leben, R. R. (1999). Coupled ocean-atmosphere dynamics in the Indian Ocean during 1997–98. *Nature, London, 401*, 356–359.

Weller, R. A., Baumgartner, M. A., Josey, S. A., Fischer, A. S., & Kindle, J. C. (1998). Atmospheric forcing in the Arabian Sea during 1994–1995: observations and comparisons with climatology and models. *Deep-Sea Research, 45*, 1961–1999.

Wyrtki, K. (1971). *Oceanographic atlas of the International Indian Ocean Expedition*. Washington, DC: National Science Foundation (531 pp.).

Wyrtki, K. (1973). An equatorial jet in the Indian Ocean. *Science, 181*, 262–264.

Xie, S. P., Annamalai, H., Schott, F. A., & McCreary, J. (2002). Origin and predictability of time-space structure and mechanisms for South Indian Ocean climate variability. *Journal of Climate, 15*, 864–15878.

You, Y., & Tomczak, M. (1993). Thermocline circulation and ventilation in the Indian Ocean derived from water mass analysis. *Deep-Sea Research I, 40*, 13–56.

Yu, L. S., & Rienecker, M. M. (1999). Mechanisms for the Indian Ocean warming during the 1997–98 El Niño. *Geophysical Research Letters, 26*, 735–738.

Yu, L., & Rienecker, M. M. (2000). The Indian Ocean warming of 1997–98 and its relation to ENSO. *Journal of Geophysical Research, 105*, 16923–16939.

Zhang, H. -M., & Talley, L. D. (1998). Heat and buoyancy budgets and mixing rates in the upper thermocline of the Indian and Global Oceans. *Journal of Physical Oceanography, 28*, 1961–1978.